JOURNAL OF MATERIALS SCIENCE 41 (2006) 177–198

Solid freeform fabrication of piezoelectric sensors and actuators

A. SAFARI*, M. ALLAHVERDI, E. K. AKDOGAN
Department of Materials Science and Engineering, Rutgers-The State University of New Jersey, Piscataway, New Jersey 08854, U.S.A.
E-mail: safari@rci.rutgers.edu

The last two decades have witnessed the proliferation piezoelectric composite transducers for an array of sensor and actuator applications. In this article, a concise summary of the major methods used in composite making, with special emphasis on Solid Freeform Fabrication (SFF), is provided. Fused Deposition of Ceramics (FDC) and Sanders Prototyping (SP) are two SFF techniques that have been utilized to make a variety of novel piezocomposites with connectivity patterns including (1-3), (3-2), (3-1), (2-2) and (3-3). The FDC technique has also been used to prototype a number of actuators such as tube arrays, spiral, oval, telescoping, and monomorph multi-material bending actuators. It has been demonstrated that SFF technology is a viable option for fabricating piezocomposite sensors and actuators with intricate geometry, unorthodox internal architecture, and complex symmetry. The salient aspects of processing of such composite sensors and actuators are summarized, and structure-processing-property relations are elaborated on. © *2006 Springer Science + Business Media, Inc.*

1. Introduction

In today's transducer technology, the use of advanced functional materials (AFM) is indispensable. Such advanced functional materials are required to perform several tasks that produce a useful correlation or feedback mechanism in a transducer system. Piezoelectrics and electrostrictors inherently possess both direct (sensing) and converse (actuation) effects. A piezoelectric/electrostrictive sensor converts a mechanical input (displacement or force) into a measurable electrical quantity by means of piezoelectric/electrostrictive effect. Alternatively, the actuator converts the input electrical signal into displacement or force. As a consequence, sensing and actuation functions can exist in tandem in a given transducer design by the intelligent use of such materials. Piezoelectrics and electrostrictors, therefore, are AFM that constitute the backbone of modern transducer technology [1].

The generic definition of an electromechanical transducer is "A device that converts electrical energy into mechanical vibration and vice versa by utilizing piezoelectricity or electrostriction" [2]. The direct piezoelectric effect enables a transducer to function as a passive sound receiver or as a pickup by the conversion of acoustic energy into an electrical signal. Applications in which such electromechanical transducers are used include hydrophones for under water low frequency noise detection and microphones. On the other hand, the converse piezoelectric effect permits a transducer to act as an active sound transmitter or a loudspeaker. A transducer can also perform both active and passive functions quasi-simultaneously in the so-called pulse-echo mode. In this mode of operation, the transducer element emits an acoustic wave into the medium of interest, and also senses the echoes reflected back onto it. Such echoes are produced when sound waves are reflected back from an interface (boundary) between two substances of different acoustic impedances. The magnitude of the echo is proportional to the acoustic impedance mismatch between the two materials forming the interface. Electrostrictive materials, on the other hand, can be used as an actuator since the strain is coupled to the applied field quadratically. Such materials have also been used as sensors where the change in permittity with applied stress constitutes the mechanism for sensing.

*Author to whom all correspondence should be addressed.
0022-2461 © *2006 Springer Science + Business Media, Inc.*
DOI: 10.1007/s10853-005-6062-x

The design and fabrication of composite materials opens new avenues to optimizing the electrical, magnetic and mechanical properties for specific application. Properties, which are otherwise impossible to achieve with constituent materials in single-phase fashion, can be synthesized by the use of several connectivity patterns. Piezoelectric composites originated from this line of reasoning so as to maximize the input and output responses of an electromechanical transducer. For instance, in the context of electromechanical transducers, one may wish to maximize the piezoelectric sensitivity, minimize the density to obtain a good acoustic matching with water, and also make the transducer mechanically flexible to conform to a curved surface. These properties are mutually exclusive; and Mother Nature does not provide us with single-phase materials that simultaneously satisfy such requirements. Thus, in many applications, one might meet conflicting design requirements by combining the most useful properties of two or more phases through the effective use of translational symmetry, i.e. the composite approach.

This review article focuses on the development of piezoelectric ceramic-polymer composites, with special emphasis on solid freeform fabrication (SFF). This advanced fabrication method brings unique degrees of freedom to composite-making, which is likely to set the stage for the prototyping of next generation piezoelectric composites in the twenty-first century.

2. Piezoelectric ceramic/polymer composites

2.1. Piezoelectric ceramics

The perovskite family comprises the largest class of piezoelectric ceramics that are used in transducer technology today [2]. Typical examples of piezoelectric ceramics with the perovskite structure include barium titanate ($BaTiO_3$), lead titanate ($PbTiO_3$), lead zirconate titanate ($Pb(Zr_xTi_{1-x})O_3$, or PZT), lead lanthanum zirconate titanate (Pb_{1-x},$La_x(Zr_yT_{1-y})_{1-x/4}O_3$, or PLZT), and lead magnesium niobate-lead titanate ($Pb(Mg_{1/3}Nb_{2/3}O_3)$-$PbTiO_3$, or PMN-PT), among others. After the independent discovery of ferroelectricity in $BaTiO_3$ ceramics in the 1940's [2] in various parts of the world, a large array of ceramic ferroelectric compounds and solid solutions have been synthesized [2–4]. Particularly, lead zirconate titanate (PZT), a binary solid solution of $PbZrO_3$ (PZ -an antiferroelectric), and PT (PT -a ferroelectric), has found widespread use in transducer technology because of its remarkable piezoelectric properties [2–4].

In addition to the monolithic ceramics, composites of piezoelectric ceramics with polymers have also been fabricated. Ceramics are less expensive and easier to fabricate than polymers or single crystals. Ceramics also have relatively high dielectric constants as compared to polymers and good electromechanical coupling coefficients. On the other hand, ceramics are disadvantageous due to their high acoustic impedance, which results in poor acoustic matching with media such as water and human tissue—the media through which it is typically transmitting or receiving a signal. The notable exception to this problem is non-destructive testing of materials (NDT), where the impedance of the ceramic can be matched to that of a metal such as steel with relative ease. In addition, ceramics exhibit high stiffness and brittleness; and cannot be formed onto curved surfaces, which contributes to limited design flexibility in a given transducer. Finally, the electromechanical resonances of piezoelectric ceramics give rise to a high degree of noise, which is an unwanted artifact in the context of transducer engineering. The best compromise in properties can be obtained by the judicious combination of piezoelectric ceramics and polymers. Piezoelectric ceramic/polymer composites possess high electromechanical coupling, low acoustic impedance, fewer spurious modes, and an intermediate dielectric constant. Moreover, composites are flexible, and are moderately priced.

Recently, there has been a growing interest in high Curie temperature systems, with special emphasis on single crystals. Materials such as lead metaniobate ($PbNb_2O_6$) [5, 6], or relaxor systems such as $Pb(Sc_{1/2}Nb_{1/2})O_3$-$PbTiO_3$ [7–11], $Pb(In_{1/2}Nb_{1/2})O_3$-$PbTiO_3$ [12], and $Pb(Yb_{1/2}Nb_{1/2})O_3$-$PbTiO_3$ [12–15] have been investigated, among others. Also, compositions in the $(1-2\times)BiScO_3-\times PbTiO_3$ ferroelectric family were studied [16–20]. The major driver for this line of research in ferroelectric materials is the sensor/actuator needs of the automotive industry.

Of very current interest is the development of non lead-based piezoelectric materials with properties comparable to that of PZT. New regulations appertaining to the use of lead-based materials in regard to environmental pollution as well as health concerns that will go in effect as early as 2007 have been the major driving force behind research activity for such piezoelectric materials in Europe and Japan. Very recently, new lead-free morphotropic phase boundary compositions of alkaline-based niobate piezoelectric solid solutions such as the $(K,Na)NbO_3$–$LiTaO_3$–$LiSbO_3$) system have been reported, whose properties are as good as PZT, especially when the material has a ⟨100⟩ texture [21].

Therefore, it is to be expected that the research in ferroelectric materials will be geared towards non-lead based materials in the future in an effort to obtain properties exceeding that of PZT along with a high transition temperature.

2.2. Connectivity patterns of piezocomposites

The arrangement of the phases comprising a composite dictate the field patterns inside the composite, which in turn, govern the electromechanical properties. A

system that allows one to codify the manner in which the individual phases are self-connected (continuous) was first proposed by Newnham *et al*. [22, 23]. There are ten connectivity patterns for a two-phase (diphasic) system, where each phase could be continuous in zero, one, two or three-dimensions as illustrated in Fig. 1.

The internationally accepted nomenclature to describe such composites is (0-0), (0-1), (0-2), (0-3), (1-1), (1-2), (2-2), (1-3), (2-3) and (3-3). The first digit within the parentheses refers to the number of dimensions of connectivity for the piezoelectrically active phase, while the latter is used for the inactive polymer phase. The polymer phase is virtually always chosen to be inactive since the purpose here is to reduce the acoustic impedance and dielectric permittivity, and not to contribute to the emission of acoustic energy. An array of piezoelectric ceramic/polymer composites have been developed based on the connectivity concept, as shown in Fig. 2 [22, 23].

Previous research has unequivocally shown that these composites exhibit superior piezoelectric properties in comparison to single-phase piezoelectric ceramics for transducer applications. In the following section, we will discuss the means by which such composites can be brought to life.

2.3. Fabrication techniques of piezoelectric composites

Various processing techniques have been utilized to fabricate piezoelectric composites. The processing techniques that found widespread acceptance include dice and fill [24, 25], extrusion [24], injection molding [26–29], lost mold [30–39], tape lamination [40–44], dielectrophoresis [45, 46], relic processing [41–43], laser or ultrasonic cutting [47–49], jet machining [33–37], reticulation [50, 51], and co-extrusion [52, 53] etc. Among these, the dice and fill, injection molding and lost mold techniques are the

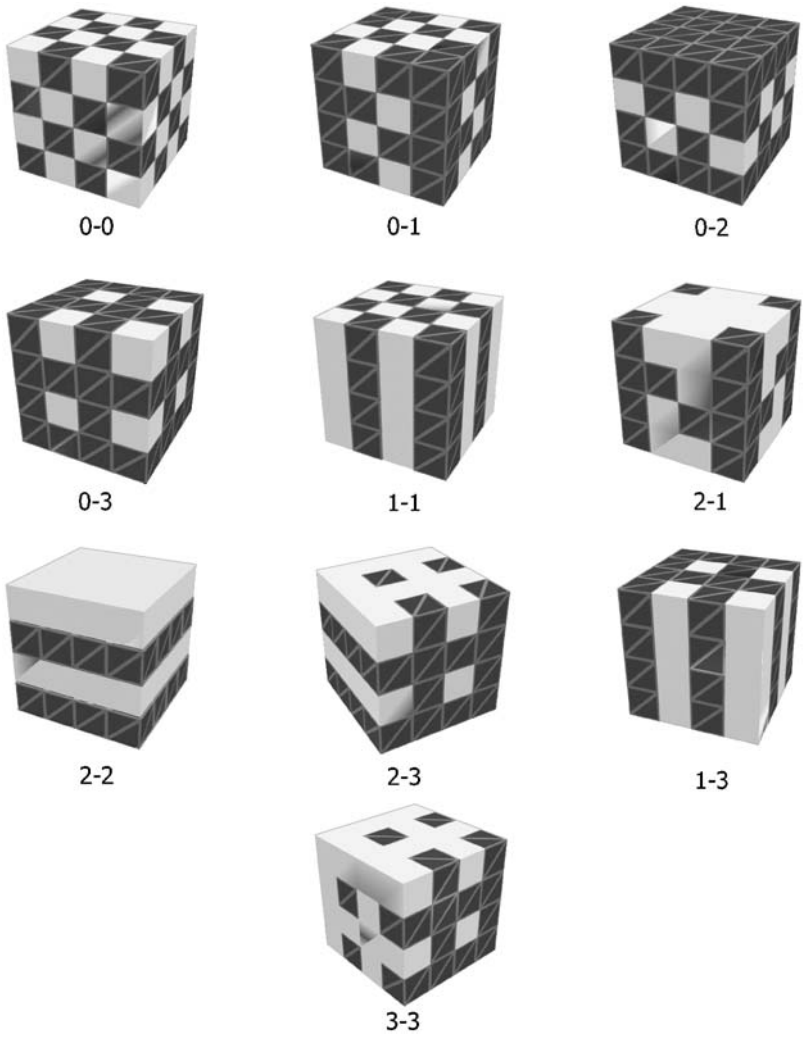

Figure 1 Connectivity families for diphasic composites. Note that the total number of connectivity patters arising from the 10 families depicted is 16 due to permutations involved in families {1-0}, {0-2}, {0-3}, {2-1}, {2-3}, {1-3}.

popular methods used for making composites on a commercial basis. Moreover, in the 1990's solid freeform fabrication techniques have also been proposed to make various piezocomposites with complex design and hierarchy, and a series of composites have been successfully prototyped.

Dice and fill method

The dice and fill method involves making a series of parallel cuts on a sintered piezoelectric block whereby a (2-2) connectivity pattern is created. If the diced sintered piezoelectric block (2-2 connectivity) is rotated by 90° and then further cut, (1-3) connectivity can be imparted to the composite. The diced ceramic block, which is still attached to the ceramic base, is backfilled with an epoxy, and then the base ceramic support is removed by polishing. The grain size of the sintered block to be cut has a strong impact on the ceramic fineness one can achieve in the dicing process—the smaller the grain size, the better the machinability. The simplicity of this method, in conjunction with readily available CAD-based wafer dicing systems, has made it very popular for fabricating (2-2) and (1-3) piezocomposite arrays for transducer applications, in general, and medical imaging applications in particular [54, 55].

Lost mold method

Skinner *et al*. and Rittenmeyer *et al*. were the first who proposed and implemented the so-called lost mold technique to fabricate (3-3) composites [56]. Siemens Inc. of Germany has also carried out pioneering work on the lost mold technique for fabricating piezoelectric composites by using a plastic mold manufactured by the LIGA (lithography, galvano-forming and plastic molding) process [31]. In the Siemens process, the plastic mold of the desired structure is filled with piezoelectric slurry. After drying, the mold is burned out and the structure sintered to >98% of the X-ray density. Composites incorporating rods with various sizes, shape and spacing could be straightforwardly made with the lost mold method, making it a very attractive process. However, the inability to rapidly prototype samples is a major drawback of this technique. Furthermore, the LIGA process is also expensive and time consuming, albeit highly accurate and of high resolution [30, 36].

Injection molding

The injection molding process is very suitable for making fine scale (2-2) and (1-3) ceramic structures with relative ease. The production of preforms with (2-2) sintered sheet composites as fine as 25-m, and (1-3) PZT rods as fine as 30–40-m in diameter has been reported by this technique [28]. Injection molding can also be used to make composites with a variety of rod sizes, shapes and spacing. The major advantages of this technique are the low material waste, flexibility with respect to the transducer design and a low cost per part. The limitation of this processing

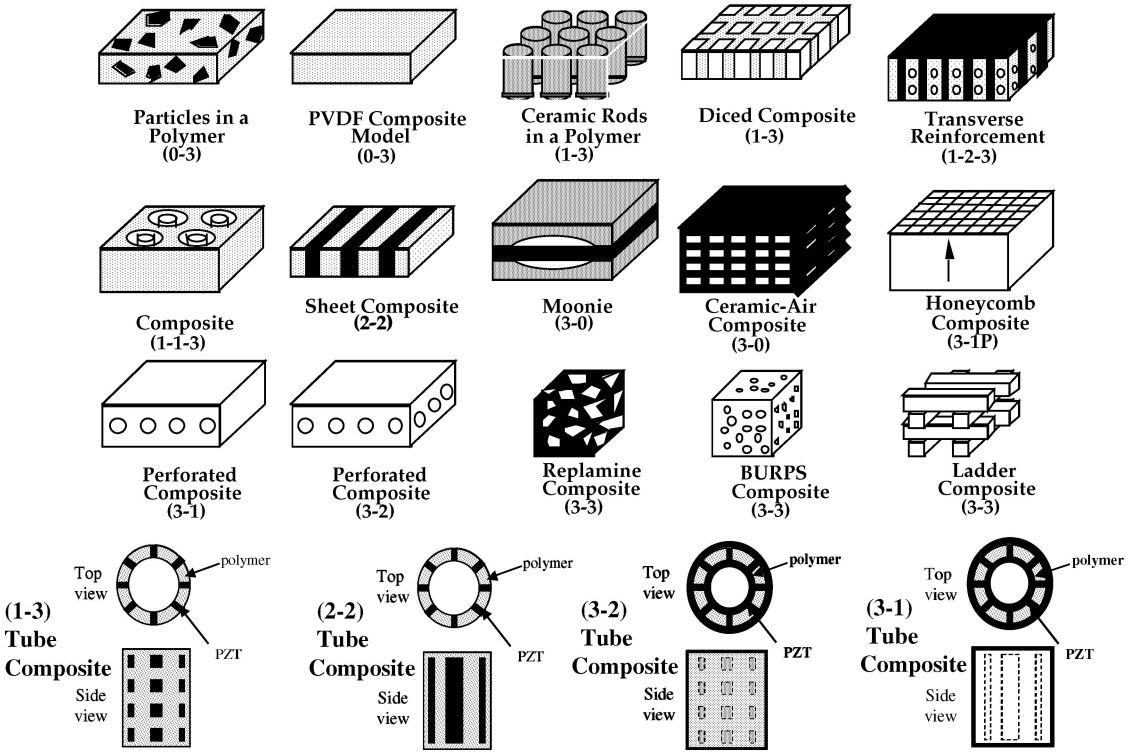

Figure 2 Schematic showing selected composites with various connectivity patterns that have been realized in the past twenty-five years.

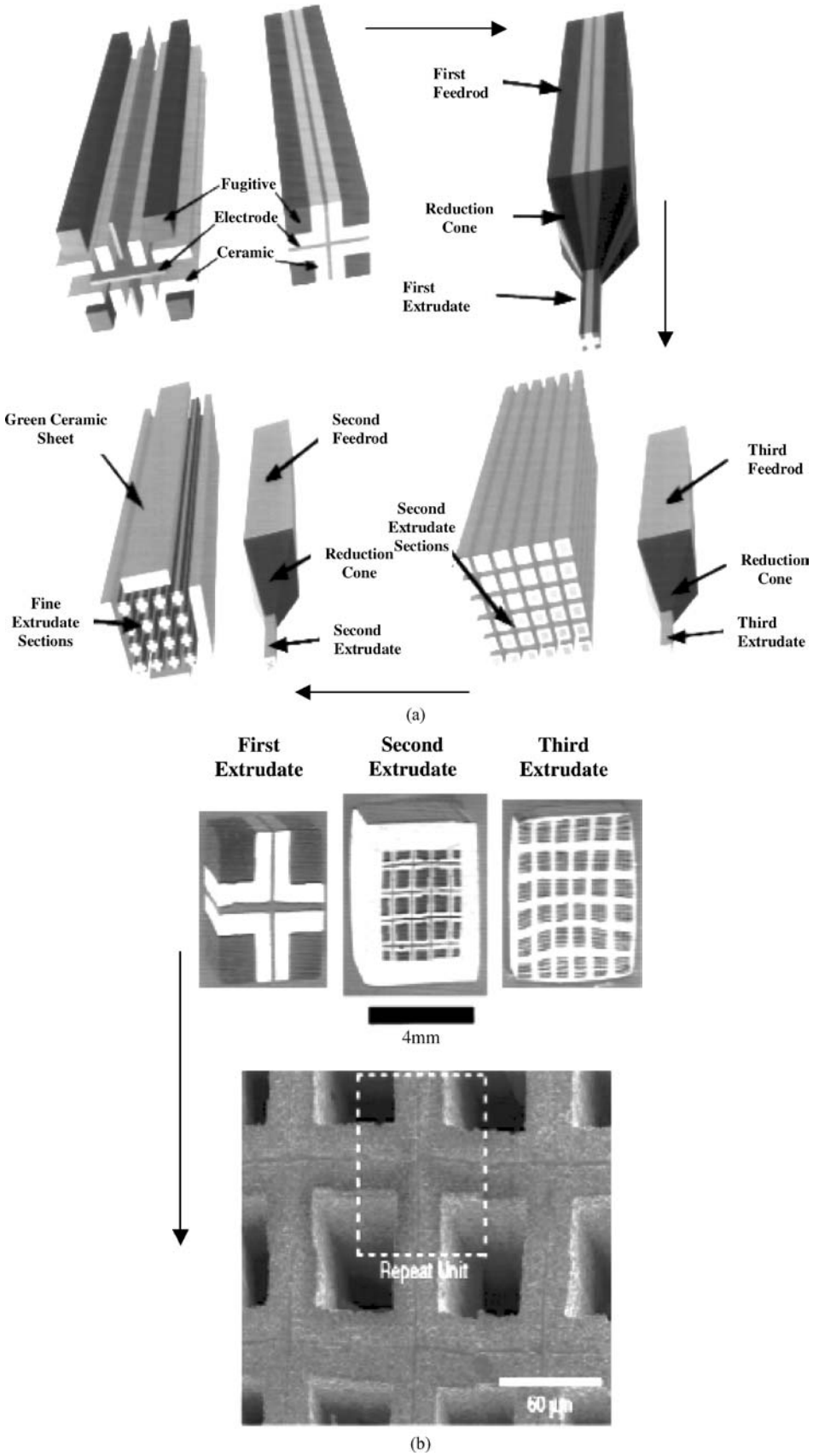

Figure 3 (a) Stepwise reduction in size by Micro-Fabrication by Co-Extrusion (MFCX), (b) cross-sectional view of the extrudates after each reduction step, and the resultant sintered microstructure.

method is the time and cost associated with making the mold. However, significant strides have been made to circumvent such problems associated with the lost mold method [26–29]. Materials Systems Incorporated (MSI) has adapted injection molding to produce net shape piezoceramics, greatly facilitating the manufacturing of large volumes of complex ceramic parts for underwater transducer applications, among others [57].

Tape casting

Tape casting has been effectively used for fabricating (2-2) composites. High frequency ultrasound transducers (>20 MHz) have been demonstrated using stacked tapes of PZT and polymer [54, 55]. With today's tape casting technology, very thin tapes (down to a several microns) can be cast, allowing manufacture of transducers for high frequency operation in high-resolution medical imaging. In addition to (2-2) composites, composites with (2-0-2) connectivity were also fabricated using PZT tapes and polymer mixed with different types of ceramic powders [59]. Other piezocomposites such as (1-3) can be made using stacked tapes and dicing. Multilayer composites with (2-2) and (1-3) connectivity patterns have also been fabricated using piezoelectric and conductive tapes [60]. Superior signal to noise ratios is within the realm of possibility in such multi-layered composites, and therefore offer high resolution capability to ultrasonic transducers [61].

Microfabrication by coextrusion

Recently, Halloran *et al.* [62, 63] developed a microfabrication by coextursion (MFCX) process, which involves forcing a thermoplastic ceramic extrusion compound through a die of a given reduction ratio. By assembling an extrusion feedrod from a shaped ceramic compound with space-filling fugitive compound, objects with complex shapes can be fabricated as shown in Fig. 3a. After each reduction state, extrudates are assembled into a feedrod and extruded again, reducing the size and multiplying the number of shaped objects. In this process, the size of the feature of interest can significantly be reduced with consecutive extrusions.

In Fig. 3b, a piezoelectric (PMN-PT) array with a final spatial resolution of 60 μm, as fabricated by MFCX, is depicted. The process has the potential for fabricating objects in the 10 μm size range [62, 63]. Therefore, the size of the features produced by MFCX is comparable to those produced using the "lost mold" technique, synchrotron radiation lithography, and also approaches the resolution realized by micromolding using photolithography [62, 63].

Solid freeform fabrication (SFF)

While the traditional ceramic processing techniques described thus far have proven to be effective for making composites with simple connectivity patterns, none of them permit the fabrication of composites with complex internal hierarchy and symmetry. The advent of a new manufacturing/prototyping technique to fabricate polymer, ceramic and metal components with very high design flexibility for novel structures, and fast prototyping is, therefore, needed. Solid Freeform Fabrication (SFF), an emerging technology that provides an integrated way of manufacturing 3-D components from computer aided design (CAD) files, arose from the concept of additive processing—a processes by which an arbitrary 3-D structure is made by cumulative deposition of material, without using any hard tooling, dies, molds, or machining operations [64–69].

In the mid-1990's, several SFF methods have been developed to fabricate polymer, metal or ceramic structures on a fixtureless platform, directly from a CAD file. Some of these techniques are designed to produce large parts with a fast output rate, and with modest surface finish. On the other hand, some of SFF techniques target markets where a very high resolution and a good surface finish are very critical. SFF or rapid prototyping methods that have found commercial success include Stereolithography (SLA, 3-D Systems Inc.) [68, 70, 71], Fused Deposition Modeling (FDM, Stratasys Inc.) [64–66], Selective Laser Sintering (SLS, DTM Corp.) [68], Laminated Object Manufacturing (LOM, Helisys Inc.) [72, 73], 3-D Printing (3-DP, Soligen Inc.) [74], Robocasting (Sandia National Labs) [74, 75], and Sanders Prototyping (SP, Sanders Prototyping Inc.) [76]. Most of these techniques are designed to manufacture net shape polymer parts for form-fitting applications and design verification. However, some are also capable of manufacturing metal or ceramic parts as exemplified by the Rutgers Fused Deposition of Ceramics (FDC) and Fused Deposition of Multi-Materials (FDMM) processes [77].

All SFF techniques begin with a common approach. Firstly, a CAD data description of the desired component is prepared. Secondly, a surface file (a.k.a. stl file) is created from the CAD file, which is later input to the manufacturing system. Thirdly, the stl file is converted into cross sectional slices, or a slice file, in which each slice can be uniquely defined about its build strategy by varying the tool path. The slices collectively define the shape of the part. And finally, the information appertaining to each slice (i.e., toolpath) is then transmitted in a layer-by-layer fashion to the SFF machine. As shown in Fig. 4, where an example from the FDC process is shown, the lowering of the fixtureless platform by one slice thickness in the Z-direction follows the completion of each layer. Subsequent layers are built on top of the preceding one in a sequential manner, and the process is repeated until the whole part is finished. The sequential or layered approach

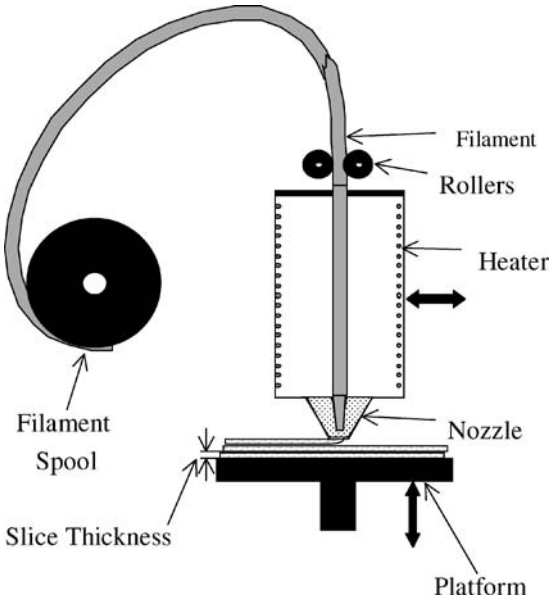

Figure 4 Schematic showing the layer-by-layer fabrication in Fused Deposition of Ceramics (FDC).

of manufacturing a 3-D object of arbitrary shape is indeed the very quintessential feature of SFF. In the Fused Deposition of Multiple Materials (FDMM) process, the same approach is pursued as in the FDC process; however, a multi-head assembly is used instead of a single head assembly. The multi-head assembly enables one to build 3D structures comprising two or more materials in a sequential fashion. While the FDMM process offers great flexibility in the design and fabrication of multi-material preforms, co-densification is a major challenge due to the differential shrinkage of in each layer. However, judicious materials selection as well as the fine-tuning of the solids loading in the filament feedstock can circumvent the aforementioned difficulty [77].

Ceserano *et al*. [78] developed the so-called Robocasting process –another near-net-shape processing method that is member of the greater SFF family of processes. Computer controlled layer-by-layer extrusion of colloidal slurries is accomplished in Robocasting. The liquid carrier is usually water, with some minor additions of dispersants and organic binders to form pastes with a plastic consistency suitable for extrusion. It has been recently shown that Robocasting could effectively be used to create complex piezoelectric lattices, which could later filled with an inactive material to make composites as shown in Fig. 5.

SFF techniques provide many advantages for the manufacturing of advanced functional components. A part normally takes weeks or months to fabricate because of the time spent in fabrication of the mold, tools and machining operations etc., in a typical conventional process. The same structure, on the other hand, can be prototyped in a few days time using SFF, thereby providing reduced lead times and costs in the development of new ceramic parts. This technology also provides the ability to do cost-effective iterative designing for producing components with optimum shape and desired properties.

3. Piezoelectric composites fabricated by SFF

The feasibility of the FDC process in making piezoelectric composites was demonstrated in the fabrication of various PZT/polymer composites with different connectivity patterns. The fused deposition process was used to fabricate piezoelectric ceramic-polymer composites via two distinct processing routes: (i) Direct fused deposition of ceramics (FDC) and (ii) Indirect technique or lost mold process where polymeric molds were manufactured by FDM^{TM} as shown in Fig. 6.

In the direct processing route, FDC was used with a PZT powder loaded polymer filament as the feed material for a direct layered manufacturing of the 3D green

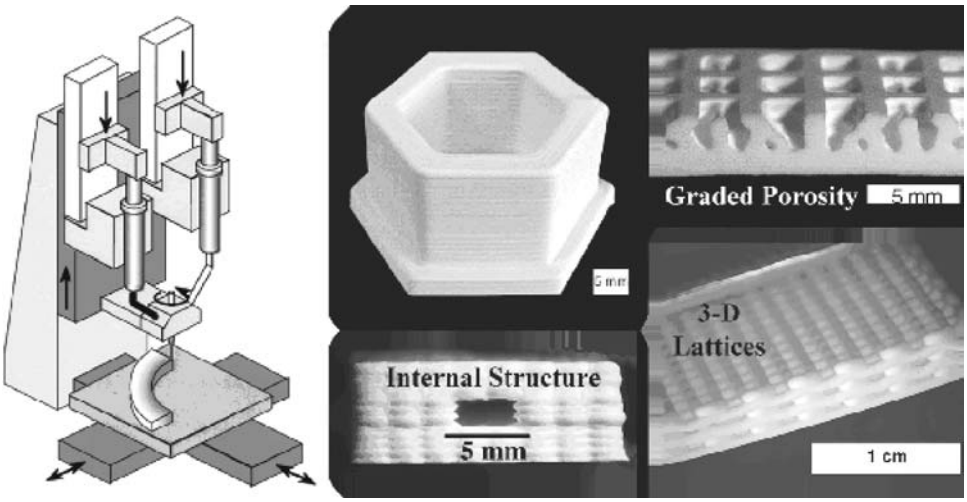

Figure 5 Three dimensional PZT lattices with (3-3) connectivity built by Robocasting.

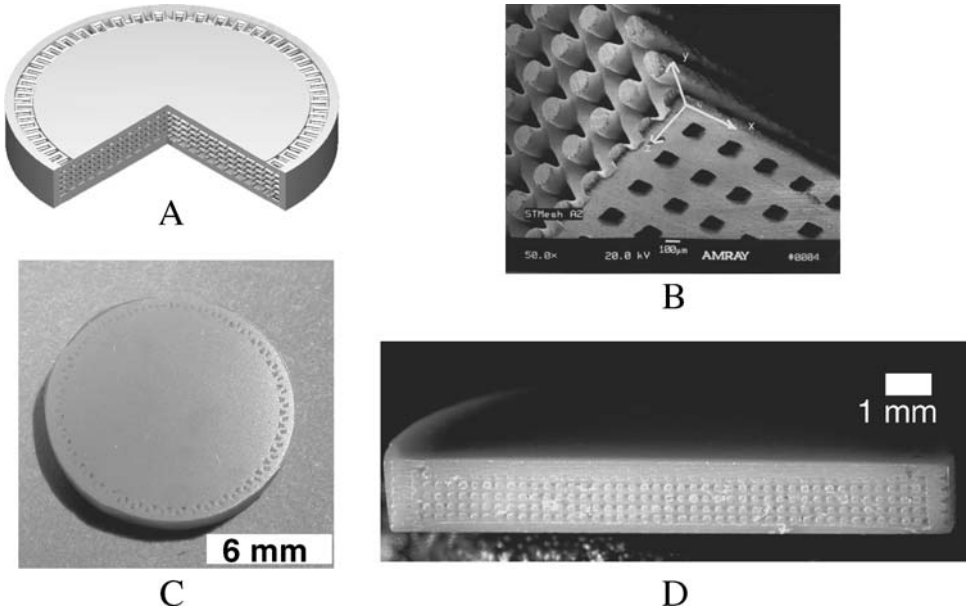

Figure 6 Piezoelectric ceramic-polymer composites via Direct fused deposition of ceramics (FDC) shown (see A & B) and Indirect technique or lost mold (C & D). Polymeric molds fabricated by FDM™.

ceramic structure. In the indirect process, Stratasys™ (Eden Prairie, MN) commercialized polymer filament was used to fabricate a mold via FDM™. A lost mold technique was then implemented to create the final structure. Embedding the ceramic structure in epoxy, followed by electroding and poling in both the indirect and direct processes obtained the composite.

Direct fused deposition of ceramics

In Fig. 7, a schematic of the direct fabrication technique is depicted on the upper path of the processing map. The optimum solids loading used in the production of filaments are typically 50–55 volume percent in a four-component thermoplastic binder system containing polymer, tackifier, wax, and plasticizer. It was found that powder pretreatment with an organic surfactant before compounding was critical in obtaining extrudable feedstock materials. Filaments of 1.78 mm in diameter are used in the process. Fused deposition of these filaments was accomplished using a 3D Modeler™ by Stratasys™, Inc. The CAD data description of the object was used to create the input file (.sml) for the 3-D Modeler™. The .sml file controls the build strategy for the part in 3D Modeler™. Samples with different volume fractions and various spacing between ceramic phases were fabricated by changing the build strategy (or the .sml file), which is due to the flexibility offered by this technique.

Indirect technique

In the indirect process, a polymer mold having the negative of the desired structure is formed via the FDM™ process using Stratasys™ commercial filament (ICW-04) and Sanders Prototyping. As shown in Fig. 7, the mold is infiltrated with the PZT slurry and then placed in a vacuum oven to ensure complete filling of the voids. The samples are then dried in an ambient atmosphere for 2 h and transferred to an oven that is maintained at 70°C. The initial slow drying step has to be included to further reduce the possibility of cracking in the slip. The thermoplastic polymer mold is evaporated during the early stages of a specifically designed binder burnout cycle. Details of each step in the process are described in the sections below.

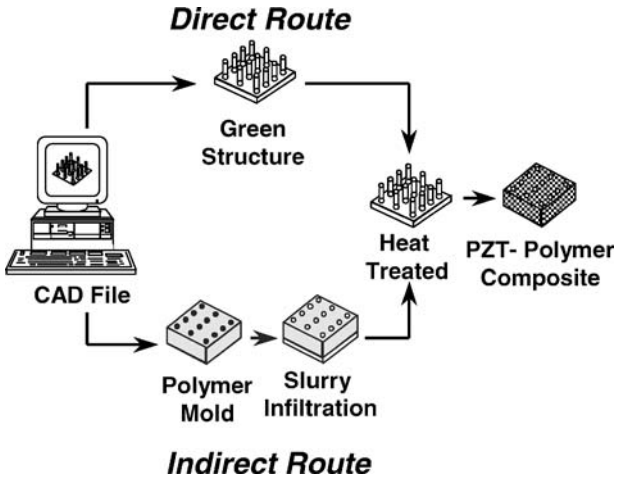

Figure 7 Schematics of the fabrication techniques used to make piezocomposites by Direct Method (*upper path*) and Indirect Method (*lower path*).

3.1. Examples of piezocomposites by SFF

Composites with (2-2) connectivity and volume fraction gradient

Regular (2-2) piezocomposites can be readily made using the dicing technique and SFF technology. However, the traditional dicing technique poses severe difficulties when one wishes to introduce a volume fraction gradient in the elevation direction of a (2-2) composite [79, 80]. That is so because the so-called kerf width has to be increased from the center to the edges, while a cutting blade with a single thickness is used in the dicing machine [81]. Furthermore, the resolution of the traditional techniques cannot be pushed under 50 μm [82]. To overcome these limitations, Panda [77] studied volume fraction gradient (VFG) (2-2) that were fabricated by the indirect lost mold route using Sanders Prototyping—a CAD-based prototyping technology. Many mathematical functions including regular, Gaussian, linear and exponential gradients were designed in order to study the effect of introducing different types of gradients along the elevation direction. The electromechanical and acoustic properties of such VFG composites were compared to those having no VFGs.

In Panda's work [77], all the VFG distributions were designed to have ~60 vol.% ceramic in that center region of the composite to obtain a high acoustic pressure output at the center. However, no further increase in the ceramic content at the center was pursued, as that would also increase the acoustic impedance difference between the central region and the edges albeit further improving the output. As a consequence, very complex matching layers would be needed for good energy transfer across the whole composite. The ceramic content in such VFG composites was gradually decreased to approximately 20% at the edges for all the types of distributions studied to ensure that the edges would act as a good receiver of ultrasonic waves due to the low dielectric constant of those regions. It should be noted that a further decrease in the total ceramic amount at the edges could further enhance the receiving sensitivity. However, this would concomitantly cause a fall in the thickness-coupling coefficient due to interference from the lateral modes, for a given ceramic element width and spacing of interest.

Fig. 8a and b show the sacrificial molds for two different functional distributions, Gaussian and linear VFG, as obtained using the Sanders prototyping technique. Throughout the structure, an air gap of 135 μm between the walls was created. Such a design enables one to ascertain that ceramic walls maintain a uniform width after slurry infiltration, as well as after subsequent heat treatment. In that particular design, the mold wall thickness was increased from 95 μm at the center to 575 μm at the edges, following the respective mathematical function. The positioning and thickness of the mold walls were very accurate with an X-Y deposition error of only $\pm$5 μm. After infiltrating PZT slurry into the molds and subsequent heat treatment, the sintered structures were embedded in Spurr epoxy. The

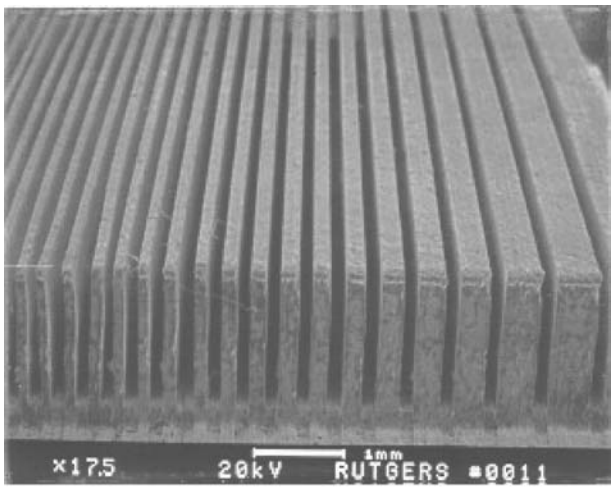

(a)

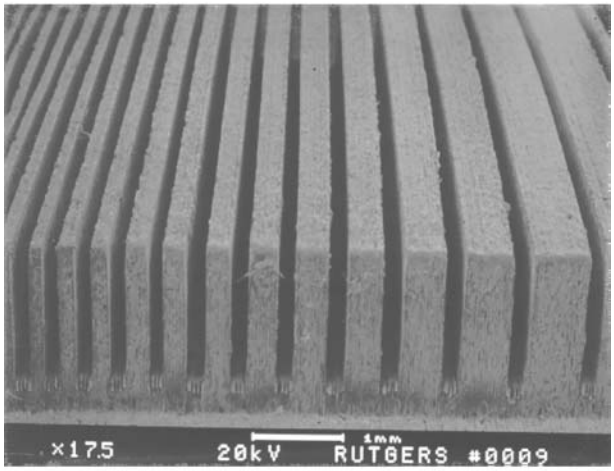

(b)

Figure 8 (a) SEM photograph showing the Sanders-built wax sacrificial polymer molds for the gaussian, and (b) linear volume fraction gradient distribution.

measurement of the dielectric properties of such linear, exponential, and regular (2-2) composites has shown that the dielectric constant was as high as 950 for the Gaussian, and 430 for the exponential design, following the total volume percent of PZT in the composite. All structures had well-discernable thickness mode resonances with k_t on the order of 66%, and moderately low values of the k_p. The high k_t in such composites was attributed to the high aspect ratio of the ceramic elements (>6), and to the soundness of the VFG design by Sanders prototyping. The longitudinal piezocharge coefficient (d_{33}) of all these composites was found to be greater than 400 pC/N.

The vibration profiles of the (2-2) composites with and without VFGs are shown in Fig. 8 as a function of the distance from the center. The pressure outputs of the VFG designs were compared with a regular (2-2) composite, which was a diced PZT-5H ceramic structure having a wall width of 220 μm and a kerf of 440 μm. The regular

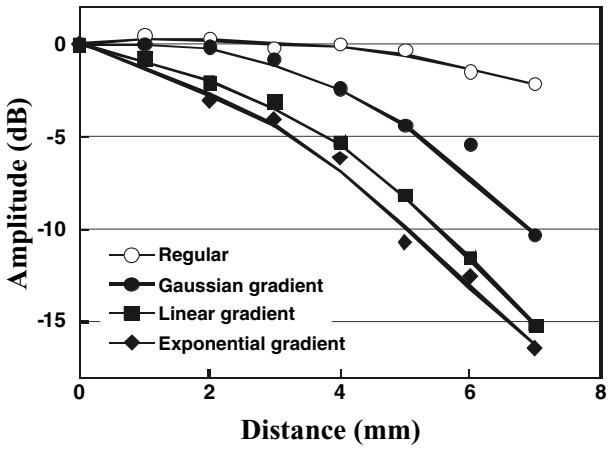

Figure 9 Graph showing the vibration amplitude profiles for 2-2 sheet composites with regular, gaussian, linear and exponential VFG distributions, as a function of the distance from the center of the structure.

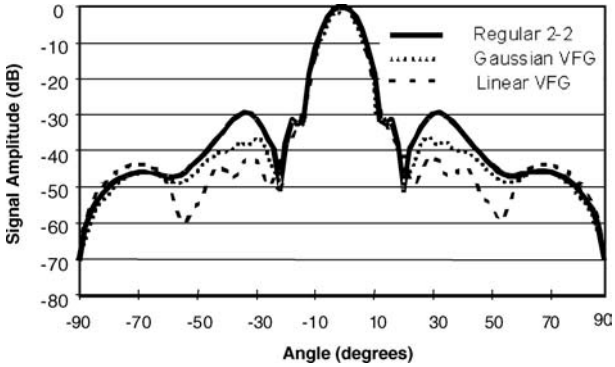

Figure 10 Predicted far field beam pattern plots for a regular, gaussian and linear VFG distribution.

design had ~33 vol.% ceramic with a d_{33} and k_t of 340 pC/N and 63%, respectively. As expected, the amplitude of the vibration for this composite did not vary much with the distance from the center, as this structure was the same everywhere. The small fall in the amplitude at the edges could be due to the edge clamping effect. On the other hand, all the VFG distributions showed a decrease in the vibration amplitude as distance from the center increased. The Gaussian VFG was designed to have a very slow decrease in ceramic volume fraction with distance from the center. The vibration amplitude observed in Fig. 9 followed a similar trend, initially remaining constant and the dropping by only −4 dB at a distance of 5 mm. Thus, this distribution was not very different from the regular (2-2) composite out to 5 mm from the center. The linear gradient showed a very smooth decline in the vibration output with distance, linearly falling to about −8 dB at a distance of 5 mm. The exponential distribution had a vibration profile that was slightly lower in amplitude than the linear distribution. It should be noted that although the ratio of the total ceramic content in the center and the edges is constant for all VFG distributions, the pressure output ratios are not similar. This could be because the 2.3 mm diameter photonic sensor probe used in the measurements of such composites shows an average reading over the probed area. Hence, the readings encompass not only the edge, but also a slightly larger region. The precise manipulation of the volume fraction within the same composite allows the control of the vibration amplitude profile to obtain the desired pressure output as seen in Fig. 10. The Gaussian vibration amplitude profile did not fall down fast and was very similar to the regular distribution. The linear or the exponential gradient showed a very smooth decrease in the vibration from the center to the edges.

Turcu *et al.* [83, 84] studied oriented (2-2) soft PZT-Epoxy composites, which were fabricated by FDC (Fig. 11). The inspiration for this study came from the modeling work of Nan et al., who investigated the effects of orientation of the ceramic phase relative to the poling directions in (0-3) and (1-3) piezocomposites [85, 86]. Nan et al.'s modeling results showed that the dielectric and piezoelectric properties of the piezocomposites with (1-3) connectivity decreased when the poling direction deviated from the orientation of the ceramic phase. In Turcu's work, the orientation angle of the ceramic phase relative to the poling direction varied in the range of 0° to 75° with 15° increments (Fig. 11) [83, 84]. The volume fraction of the ceramic phase in both composites was fixed at 0.30. It was found that the dielectric constant and piezoelectric d_{33} coefficients of both composites decreased with increasing orientation angle. However, the piezoelectric d_{31} coefficient became positive at 45° reaching a value of 150 pC/N. The relevant hydrostatic piezocharge and voltage coefficients, and the FOM of the oriented composites were calculated as shown in Figs 12 and 13, respectively [83, 84]. The data exhibit $d_h g_h$ maxima at an orientation angle of ~45°.

Composites with (3-3) Connectivity

A composite with (3-3) connectivity is comprised of two phases that mutually penetrate, and thereby form two three dimensionally self-connected networks in intimate contact. The feasibility of the FDC process for making piezoelectric composites was demonstrated in the fabrication of PZT/polymer 3-D honeycomb and ladder composites with (3-3) connectivity patterns [77].

Two scanning electron micrographs of a typical heat-treated ceramic ladder structure prepared by the direct FDC method prior to epoxy infiltration are shown in Fig. 14. The ladder structures were built by using a raster fill strategy with a fixed inter-road spacing. The consecutive layers were built 90° to each other. The volume fraction of the ceramic phase in the structure shown in Fig. 14 is approximately 70 percent, and can be varied by varying the width and spacing between the ceramic

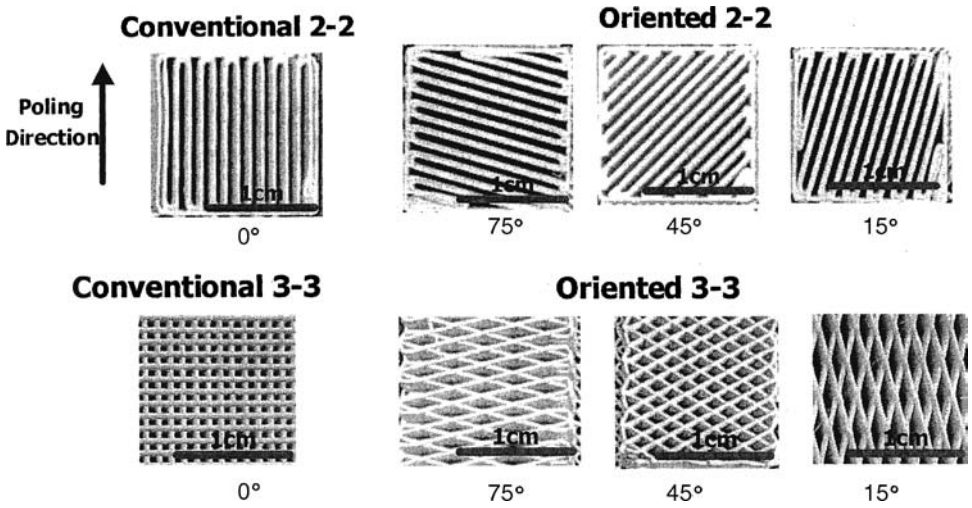

Figure 11 Oriented (2-2) and (3-3) composites fabricated by the Fused Deposition of Ceramics process.

roads. In Fig. 14, the ceramic roads are ~300 μm wide with ~800 μm center-to-center spacing. The mesoscopic structures created by FDC are very uniform with excellent unit cell repeatability, unequivocally demonstrating the superiority of the FDC process over traditional methods of composite making [77].

The indirect method was also used to fabricate 3-D honeycomb composites. The scanning electron micrographs (SEM) in Fig. 15 depict the various orientations of a typical heat-treated ceramic structure prior to epoxy infiltration from. Fig. 15a shows the top, front and side faces, while Fig. 15b shows the top and front faces. The structure consists of a 3-D lattice of "air pipes" defining the 3-D piezoelectric skeleton (matrix). The "air pipes" were created upon burning out the sacrificial polymer. By virtue of the flexibility offered by the FDC process, the diameter of the holes, the spacing and the volume fraction of the ceramic phase can be varied between the holes. In the example given in Fig. 15, the diameter of the holes is ~200 μm, with ~350 μm center-to-center uniform spacing, and the PZT content is ~25% by volume [77, 87, 88].

The dielectric constant (K_{33}) and piezocharge coefficient (d_{33}) of several 3-D honeycomb composites fabricated by the indirect method with 10–35 volume percent PZT loading is are shown in Fig. 16. An increase in K as the volume percent of PZT increased was observed, which is in conformity with mixing laws to a first approximation. It is also seen that there is an increase in d_{33} as the volume percent of PZT increases from 10 to 30. The d_{33} value then levels off at about 35 volume percent PZT, where pseudo-single phase behavior is reached [88].

Very recently in another application of SFF, namely Robocasting, it has been demonstrated that one can successfully fabricate piezoelectric composites [89]. As shown earlier in Fig. 5, composites with (3-3) connectivity have been built out of PZT, and were found to exhibit reasonable hydrostatic FOM. It was also shown that the incorporation of a faceplate in these (3-3) composites increased the FOM by approximately one order of magnitude, reaching a value of approximately 8000×10^{-15} m^2/N.

Turcu *et al.* [83, 84] studied oriented (3-3) soft PZT-Epoxy composites by FDC (Fig. 11). This CAD-based approach allowed the design of the piezoelectric "road" thickness, line spacing, composite thickness, as well as the orientation of the "roads". Testing of the said composites revealed that the piezoelectric voltage coefficient (g_{33}) showed a significant increase (about 85%) in (3-3) composites at an orientation angle of 45°. The FOM of the oriented (3-3) composite reached an extremely high value of ~$50{,}000\times10^{-15}$ m^2/N, while a more modest increase was seen for the (2-2) composites ($14{,}000\times10^{-15}$ m^2/N) as shown in Figs 12 and 13, respectively.

Radial composites

Monolithic ceramic tubes, like their planar counterparts, suffer from similar deficiencies such as high weight, high capacitance, and low figure of merit $d_h g_h$. Until recently, the fabrication of functional piezoelectric composites with radially-oriented connectivity has been difficult or impossible using conventional processing. With the advent of Rapid Prototyping, these types of composites can be fabricated with relative ease.

Radial composites with four different connectivity patterns have been fabricated using FDC and Sanders Prototyping (SP) processes. These consist of (1-3), (2-2), (3-1), and (3-2) type composites. For the purpose of simplicity, cylindrical coordinate systems are being used to designate the connectivity of each composite design. For the (1-3) type composite, the ceramic phase is continuous in only the r direction, while the polymer phase is continuous in the diameter (r), height (z), and sweep angle (θ) directions (Fig. 2). For (2-2) type composites,

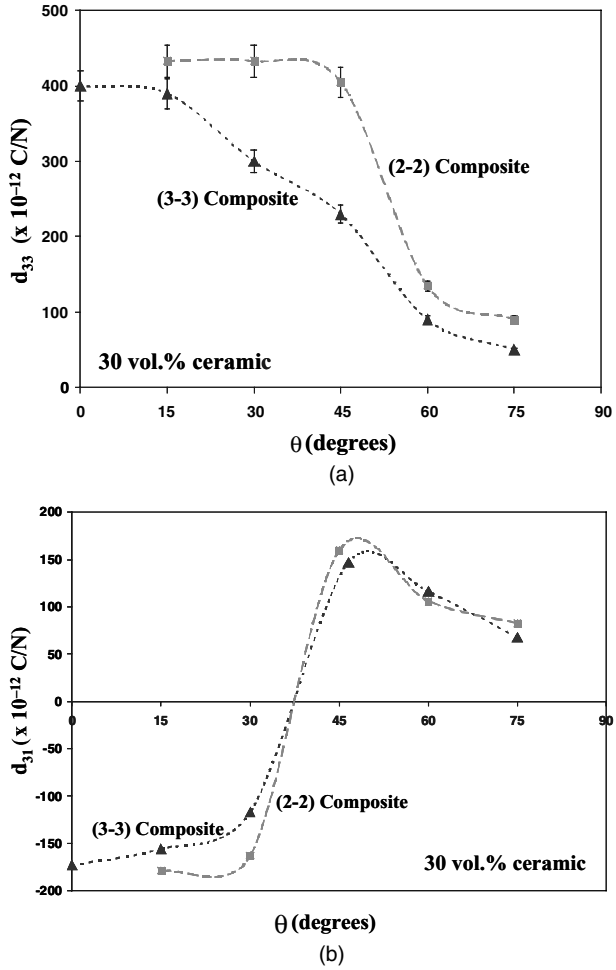

Figure 12 Piezoelectric properties of oriented (2-2) and (3-3) composites fabricated by FDC: (a) longitudinal piezostrain response, (b) transverse piezostrain response.

both the ceramic phase and the polymer phases are continuous in the r and z directions. In the case of (3-1) type composites, the ceramic phase is continuous in all three directions, while the polymer is continuous in only the z direction. Finally, for the (3-2) type composites, the ceramic phase is continuous in all three directions, while the polymer phase is continuous in the z and θ directions.

Fig. 17a and b shows the photograph of a tubular (3-1) PZT ceramic preform made using Fused Deposition of Ceramics (FDC). In this structure, the inner and outer ceramic rings are approximately 1 mm in thickness, and the ceramic sheets connecting the inner and outer rings are approximately 1 mm by 1 mm. Fig. 17c shows the picture of a (3-3) sintered ceramic made using a SP rapid prototyping system.

Curved transducers

Curved ceramic skeletons for (2-2) composite were built with 10 and 20 cm radii of curvature (Fig. 18a). Flat

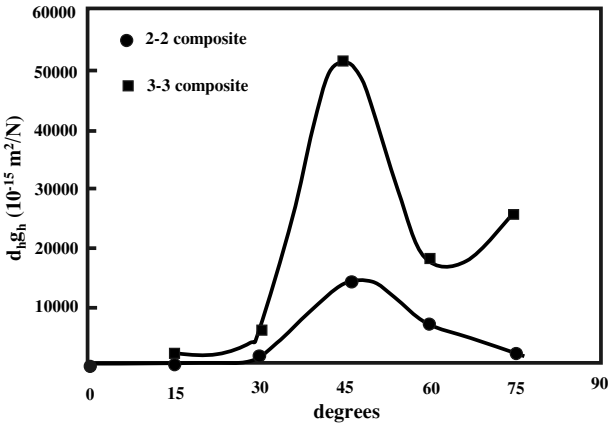

Figure 13 Effect of piezoelectric phase orientation on the figure of merit ($d_h g_h$) in (2-2) and (3-3) oriented composites made by FDC.

samples were also built for comparison of the electromechanical properties. In the FDC built green parts, the ceramic plates were 330 μm thick and the spacing between the plates was 760 μm. Physical characterization of the samples revealed that 95% of the theoretical density was achieved upon sintering. Optical micrographs of the parts in the green and sintered states were taken. Fig. 18b shows the surface roughness associated with the layer-by-layer building of the FDC technique. The slice thickness was found to be constant; however, the road width showed a significant spread in values. SEM of fracture surfaces of the sintered samples showed that good bonding occurred between the roads; no delamination was visible.

4. Piezoelectric actuators fabricated by SFF

Several piezoelectric actuators with novel designs have been made and characterized in the last few years [90–92]. It has been demonstrated that improved electromechanical properties can be achieved by tailoring the geometry and dimensions of an actuator. Ceramic processing techniques such as injection molding is costly and time-consuming to develop and prototype new actuators. Solid freeform fabrication has brought a high degree of flexibility, cost-effectiveness and speed to the field of piezoelectric actuator prototyping.

In the last ten years, SFF methods in particular FDC have been utilized to fabricate a series of piezoelectric actuators [91, 93–98]. Processing and properties of a few rapidly prototyped actuators will be reviewed with emphasis on the recent results on unimorph and multimaterial spirals and bending actuators, as well as tube actuators with curved tube walls.

4.1. Prototyped actuators

Piezoelectric actuators generate field-induced displacements that can be used in motion systems such as micro-

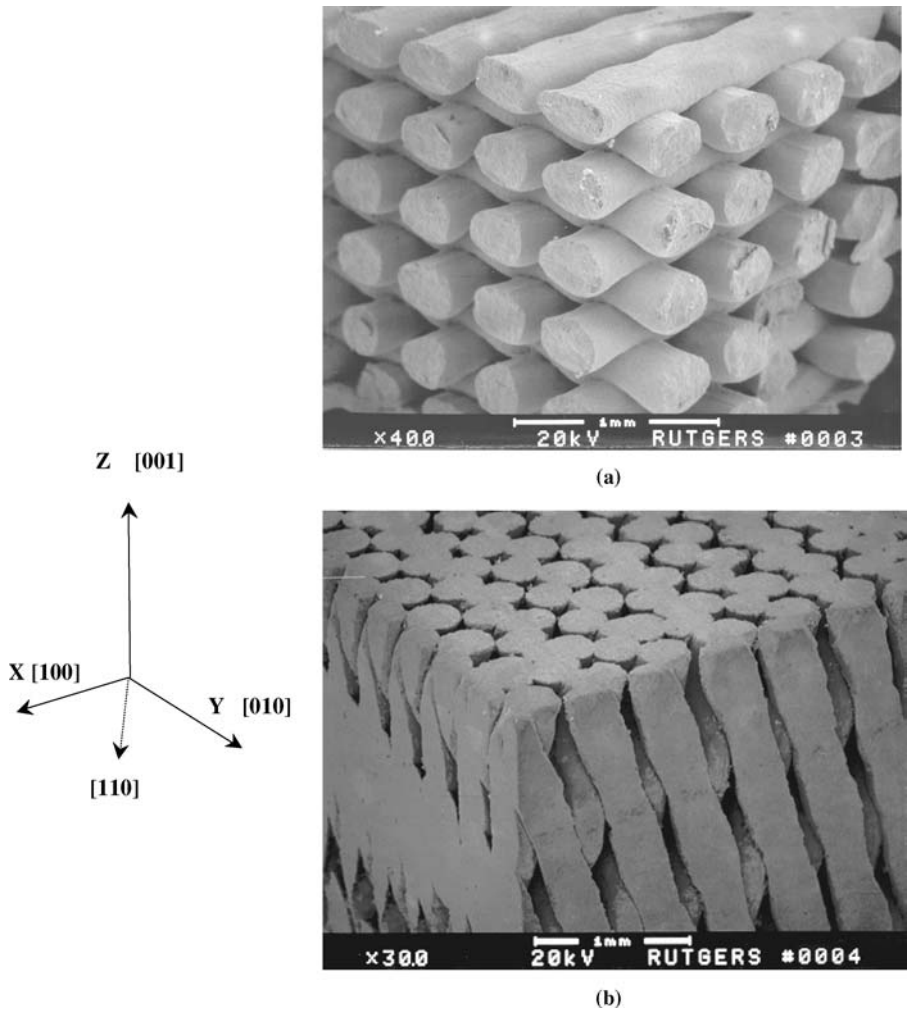

Figure 14 Ladder structure with (3-3) connectivity as obtained by FDC. Upon impregnation with polymer, a (3-3) piezoelectric ceramic/polymer is formed.

positioners, ultrasonic motors, and vibration damping. It is desirable to enhance the displacement while maintaining a reasonable amount of load bearing capability. This has been achieved by manipulating the geometry of simple shape (rod or strip) actuators into more complex geometries [1, 2, 99, 100]. For example, the axial displacement of a solid piezoelectric cylinder (rod) can be improved by replacing it with a tube of similar height and diameter. Other techniques such as the addition of a stiff inactive layer (a metal shim in unimorph and bimorph actuators) have also been utilized to improve displacement [92, 101].

Using the FDC process, a series of novel actuators have been designed and prototyped to study the effect of design/geometry on the field-induced displacement. The flexibility of FDC has allowed for the rapid fabrication of actuators with complex geometry that cannot easily be made by conventional manufacturing techniques. These actuators include spiral [2], telescoping [97], dome [98], tube [102], curved and multilayered tubes, bellows, oval, and monomorph benders [7]. Spiral and tube actuators will be briefly reviewed with the emphasis on the recent results.

Spiral actuators

Spiral actuators with a compact geometry show large field-induced strains (Fig. 19a). The application of an electric field across the spiral width induces both tangential and radial displacements, the former being much larger than the latter. It has been shown that for a PZT spiral actuator with 32 mm diameter, the tangential movement reaches 1.9 mm at ~11.6 kV/cm [97]. This is about twelve times higher than the displacement of a PZT strip of the same dimensions, which clearly shows that displacement can profoundly be enhanced by tailoring the geometry of the actuator.

In a curved geometry like spiral, there exists a slight gradient in the displacement of small elements across the thickness (Fig. 19b). This means that the displacement of an element in the outer diameter (r_o) is larger than that of

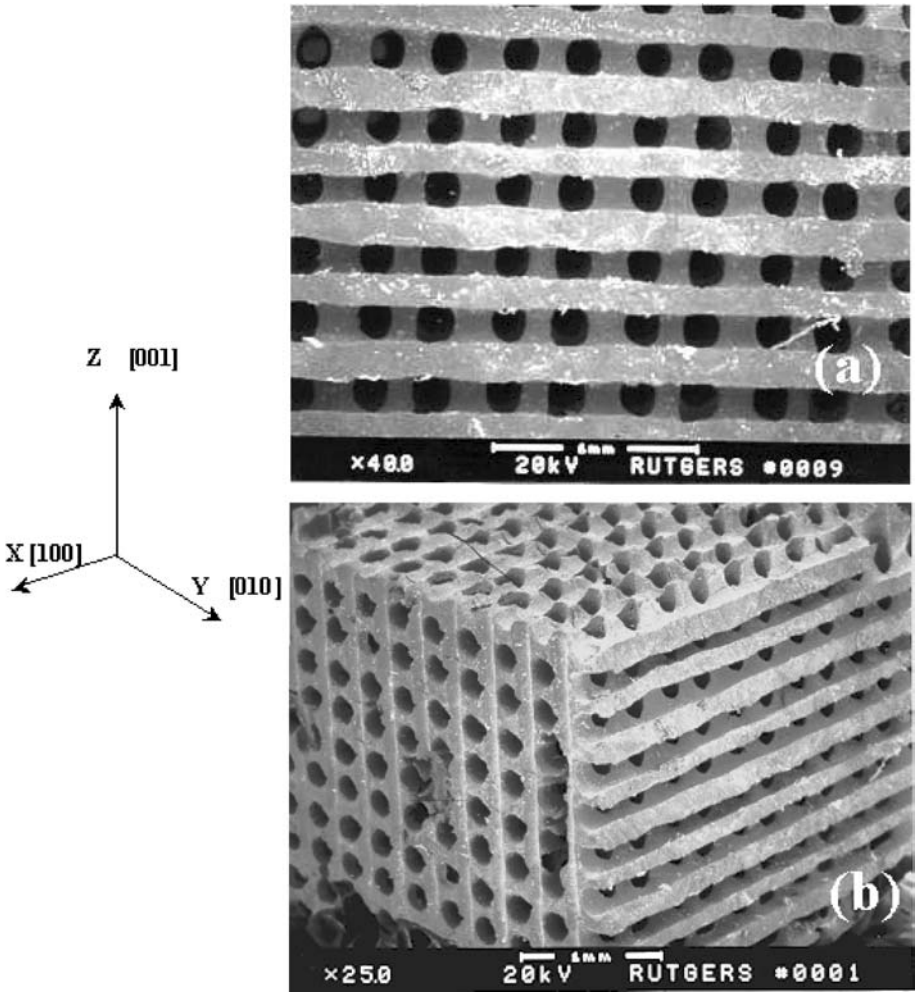

Figure 15 Honeycomb structure made out of PZT using FDC (a) front view, (b) oblique view.

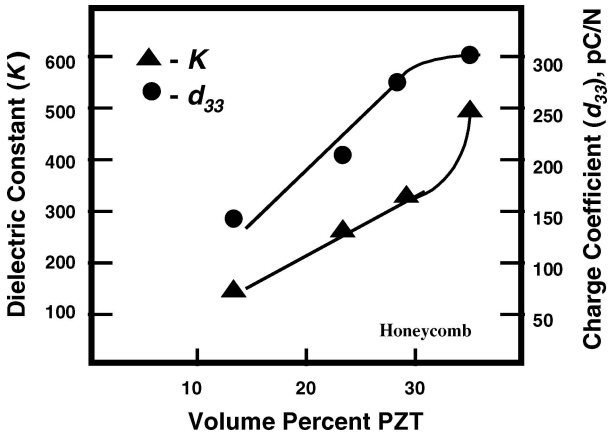

Figure 16 Variation of dielectric constant and piezocharge coefficient for a honeycomb composite with volume percent of PZT loading.

an element in the inner diameter (r_i). Such a phenomenon creates a bending moment, which leads to rotation or large tangential displacement in spirals. The large actuation of spirals is obtained at the cost of load bearing capability since the two are inversely related. For example, the blocking force for the above-mentioned spiral actuator, measured at various electric fields (1.3 to 3.3 kV/cm), is ~0.8 N [8]. Despite low blocking force, spiral actuators are of interest due to large displacement and compact geometry.

To further enhance the actuation, unimorph PZT spiral actuators have been investigated. Modeling results of spirals have suggested that asymmetric electrodes/shims can enhance the tangential displacement significantly [103]. Unimorph spirals were fabricated by attaching a stainless steel shim on the inner side of the spiral wall. In a conventional unimorph, the relative difference between the length of ceramic and metal strips under an electric field results in bending and therefore, large tip displacement. A PZT spiral actuator (width = 1.05 mm, diameter = 28.85 mm, height = 2.55 mm) with a 37.5 μm stainless steel shim was fabricated and tested. The addition of the stainless steel shim increased the tangential displacement by 200% at 850 V, as depicted in Fig. 20. This increase in displacement is analogous to the bending of a

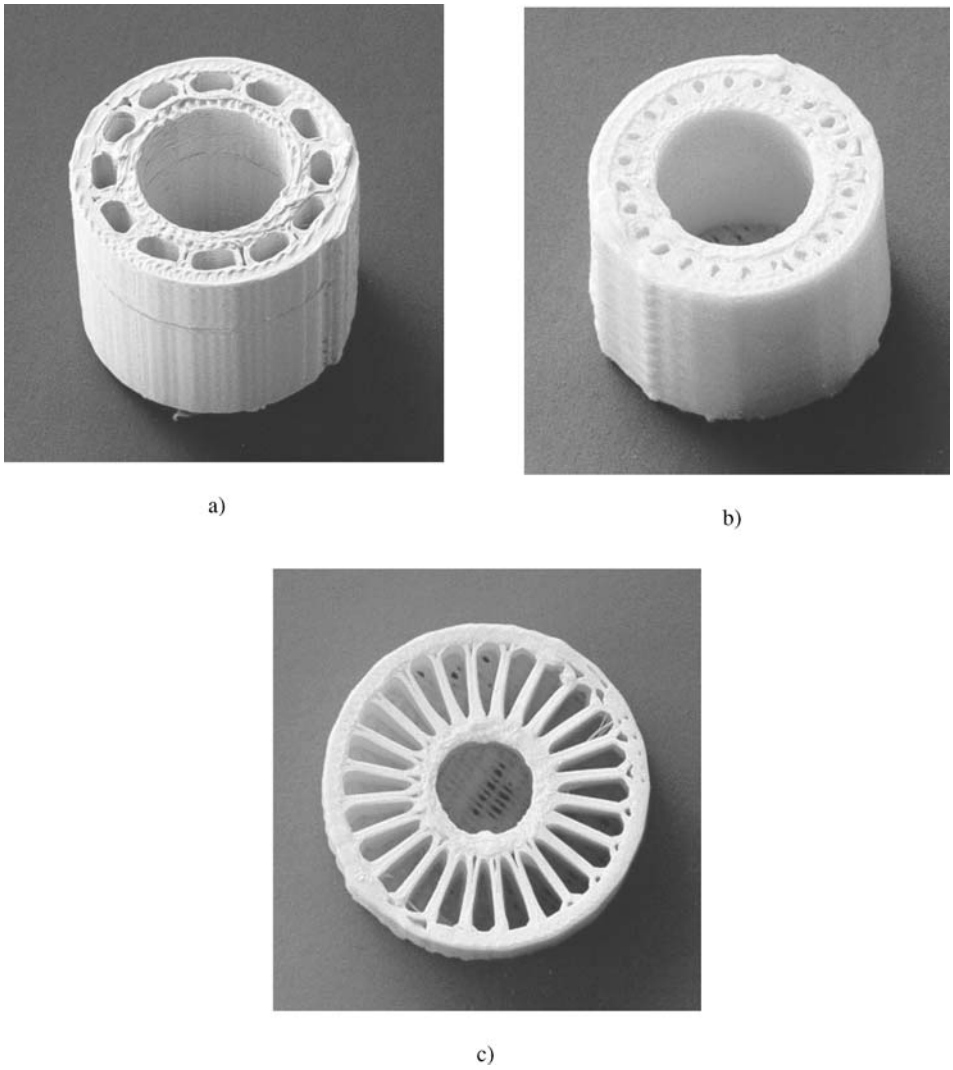

Figure 17 (a) Photograph of radial 3-1 type (design 2) hydrophone preform made via FDC, and (b) radial 3-2 type hydrophone, and (c) radial 2-2 type hydrophone.

conventional unimorph. It is also seen that the hysteresis of the unimorph spiral was much higher (e.g., about six times higher at 400 V) than the regular spiral actuator.

In another series of experiments, the tangential displacement of spirals with dissimilar ceramic strips was investigated. For this purpose, multimaterial spiral actuators consisting of one piezoelectric and one electrostrictive PMN-PT layer with the same thickness were fabricated and tested. These actuators can be driven in such a way that there is a strain gradient in the actuation between the piezoelectric and electrostrictive layers. This would further enhance the bending moment of the spiral. The multimaterial spiral actuator was designed such that the outer side of the spiral wall was the piezoelectric 0.65PMN-0.35PT layer, while the inner side of the wall was the electrostrictive 0.90PMN-0.10PT layer. Such spirals were prototyped by FDC and co-fired successfully at 1250°C for 1 h. Measurements have shown that the combined piezoelectric/electrostrictive spiral actuator yielded higher displacements than a piezoelectric actuator of similar dimensions. For example, the piezoelectric/electrostrictive actuator displaced to ~510 μm at 500 V as compared to ~200 μm for the piezoelectric actuator at the same DC biased field. The enhancement of tangential displacement was accompanied by large hysteresis of the multimaterial actuators similar to the unimorph spirals.

Tube actuators

Piezoelectric tubes are utilized for actuator (Ink Jet Printing) and sensor (1-3 piezocomposites) applications, among others [102, 103]. Tube actuators have demonstrated promising properties and have been successfully used to shift mirrors of laser resonators in scanning tunnel microscopy and atomic force microscopes.

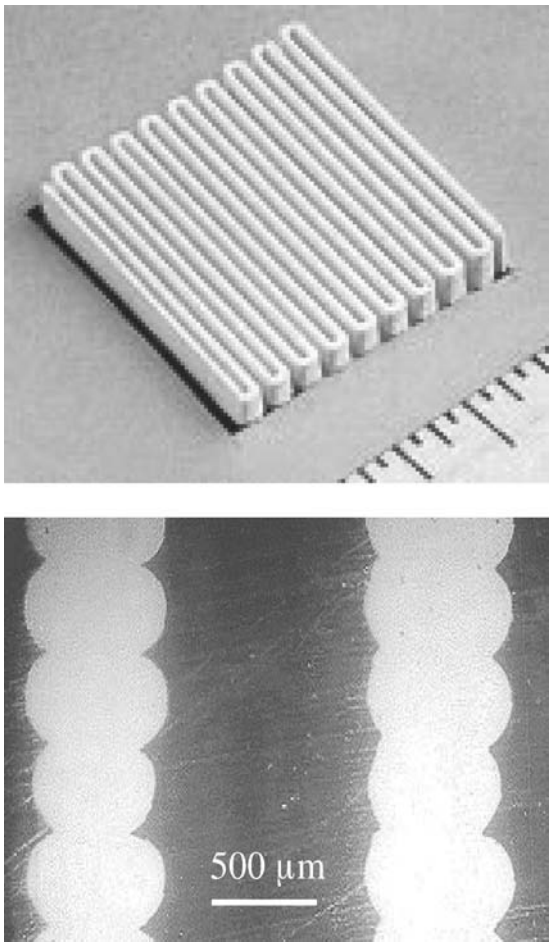

Figure 18 (a) Photograph of a curved green 2-2 PZT-5H preform. (b) Optical micrograph of the cross section of the walls of the structure.

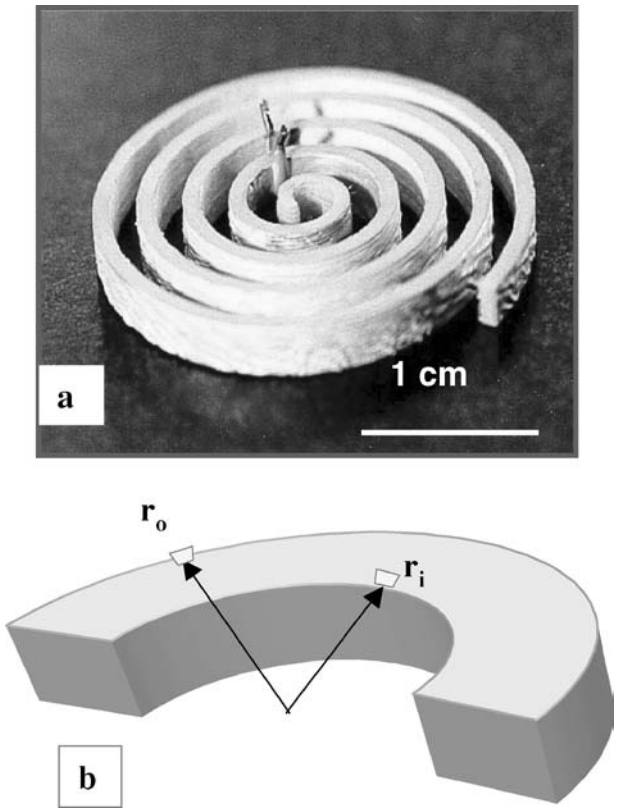

Figure 19 (a) Spiral actuator and (b) schematic of a curved piezoelectric segment, illustrating elements in the outer and inner diameters. A slight displacement gradient exist across the thickness, resulting in bending stress and segment rotation.

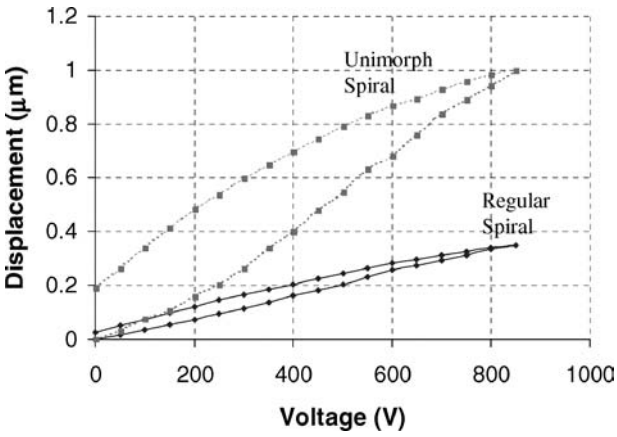

Figure 20 Displacement enhancement in PZT spiral actuator as a result of adding a 37.5 μm shim.

Single tube and tube arrays (Fig. 21a) were fabricated with various diameter, height, and wall thickness via the FDC process [102]. Tube geometry has been modified to tune properties (e.g., resonance frequency and axial displacement) for a given application. Tube actuators with zigzag wall design (bellows, Fig. 21b) have also been prototyped to study the effect of wall configuration (bellows angle) on the axial and radial displacements [104]. Comparison of bellows with the straight tubes revealed that the bellows possess up to 50% larger radial displacements, whereas their axial displacements were about 20–30% lower.

Another type of tube actuator with helical electrodes has also been investigated (Fig. 21c). Normally, the inner and outer surfaces of the tubes are electroded and the tubes are poled radially. In this manner, the actuation or sensing is based on the d_{31} coefficient. However, in the new design the electrodes are laid side by side in helical form along the tube height [105]. For such piezoelectric tubes, displacement is derived from the d_{33} coefficient, resulting in a potential improvement of more than two times in axial displacement (d_{33} / d_{31} > 2). In addition to tubes with helical electrodes, multilayer tube actuators (Fig. 21d) also benefit from the larger piezoelectric coefficient of d_{33}. Successful fabrication of these actuators depends upon the electrode materials, its thickness, and sintering conditions/atmosphere [104, 105].

It has been shown that the actuation of a piezoelectric element can be improved if a given structure is curved. For example, dome [101], RAINBOW (Reduced and

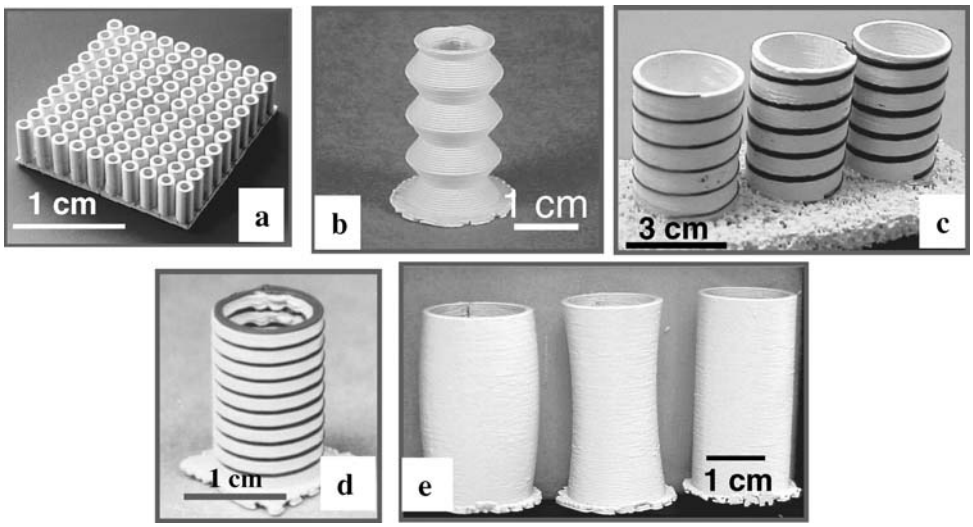

Figure 21 Various tube actuators made by the FDC process. (a) tube array, (b) bellows, (c) tubes with helical electrodes, (d) multilayer tube, and (e) tubes with curved walls.

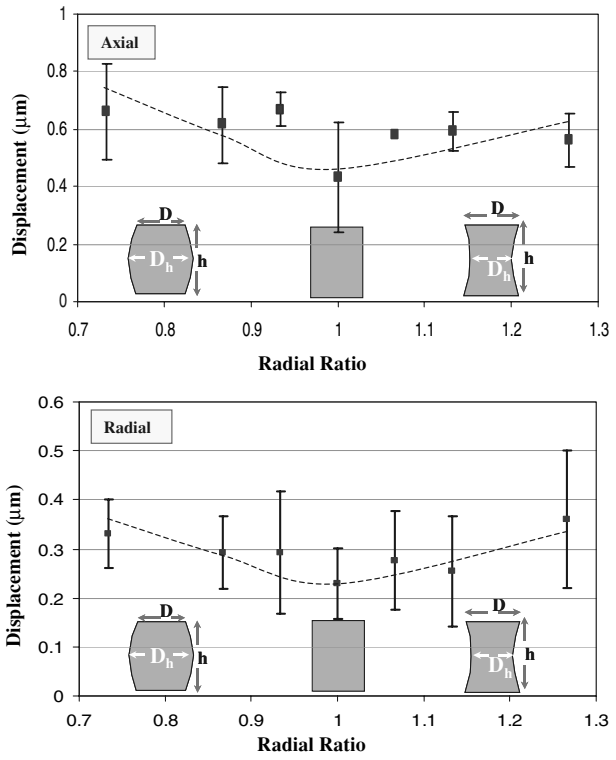

Figure 22 The effect of tube curvature on the axial (top) and radial (bottom) displacements of the tubes (radial ratio is D/Dh).

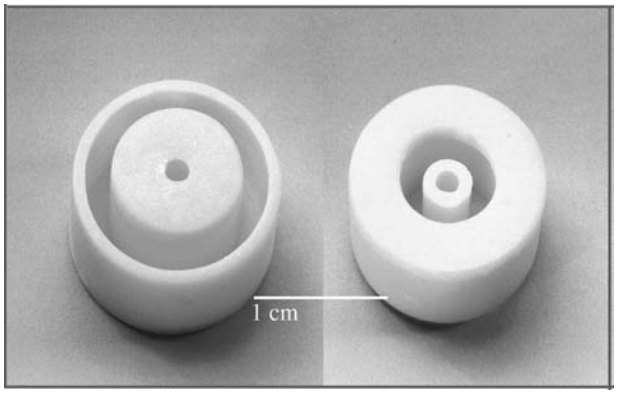

Figure 23 Photograph showing the top and bottom faces of a telescoping actuator structure.

Internally Biased Oxide Wafer [1]), and THUNDER (Thin Layer Unimorph Driver [99] actuators illustrate displacement enhancement as a result of curved geometry and internal stresses. In order to determine if curvature would have a positive impact on tube actuators, PZT tubes with curved walls (both with inward and outward curvatures, as shown in Fig. 21e, were designed, prototyped, and characterized. All the green tubes were of the same height, end diameter and wall thickness (20 , 15 , and 1 mm, respectively). The axial and radial displacements of these tubes, measured by a photonic sensor, are plotted in Fig. 22. Despite the large variation of data points, it appears that the regular (straight-walled or radial ratio of 1) tubes showed minimum displacement whereas the curved-wall tubes showed slightly larger actuations, likely due to the wall curvature. It is speculated that the constrained geometry of these actuators (tubular shape) limits the contribution of the curvature, and therefore, only slight improvement can be gained in radial and axial displacements.

Telescoping actuators

Another monolithic ceramic actuator with telescoping actuation was also fabricated by the FDC method. The device consists of interconnected PZT ceramic tubes bearing a common center with internal displacement amplification under electric field (Fig. 23). Upon the application of an

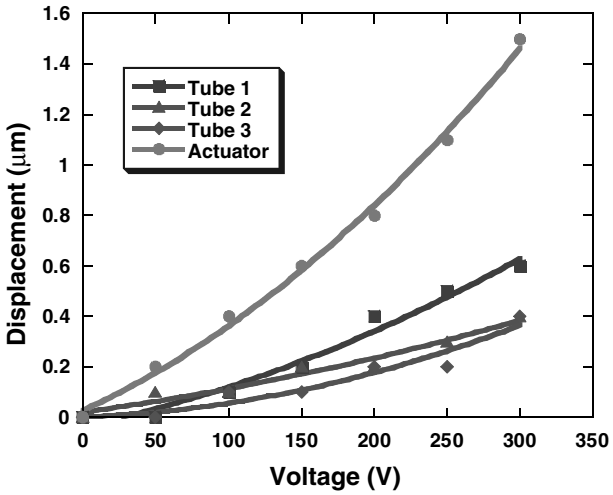

Figure 24 Field induced displacement of a telescoping actuator.

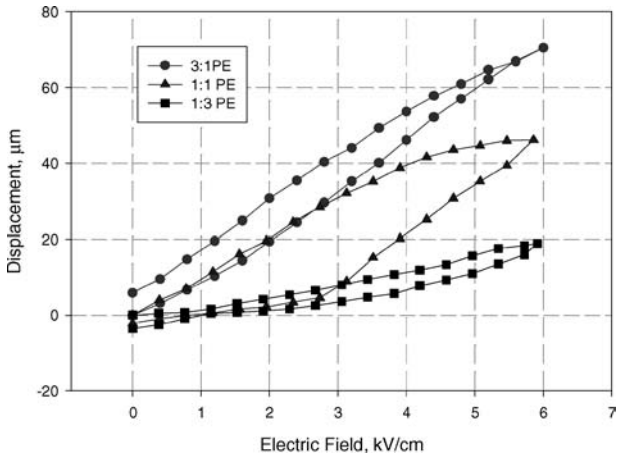

Figure 26 Displacement vs. electric field for 1:1, 1:3, and 3:1 PE monomorph (Thickness=1.26 mm).

electric field, the tubes elongate and shrink alternatively in the *z* direction, yielding a net additive displacement in the *z* direction. The telescoping actuators consist of three interconnected PZT ceramic tubes with a common center. Under applied electric field, the inner and outer tubes elongate and the middle tube shrinks in the *z* direction. The telescoping actuation of the device is the summation of actuation of all individual tubes in the actuator (Fig. 24). Therefore, increasing the number of the tubes, which are the driving component of the actuator, will further increase the displacement. Tailoring of the thickness, height, and the number of driving components of the actuator, the displacement and the exerted force of these actuators, can be altered.

Monomorph bending actuators

Monolithic multi-material monomorphs comprised of varying ratios of piezoelectric $0.65Pb(Mg_{2/3}Nb_{1/3})O_3$-$0.35PbTiO_3$ to electrostrictive $0.90Pb(Mg_{2/3}Nb_{1/3})O_3$-$0.10PbTiO_3$, have been designed and fabricated. The strain gradient between the piezoelectric and electrostrictive layers causes a bending moment to develop and therefore, the tip deflects. The schematic of piezoelectric/electrostrictive actuators is shown in Fig. 25 The relative permittivity, displacement, and polarization hysteresis were investigated for varying ratios of piezoelectric to electrostrictive material. The P-E hysteresis loop of the 1:1 sample exhibited saturation and remnant polarization slightly less than the piezoelectric PMN-PT 65/35, but higher than the electrostrictive PMN-PT 90/10.

Fig. 26 depicts the dc-displacement of 1:1, 3:1, and 1:1 monomorph actuators, respectively. The maximum tip deflection of the 1:1 monomorph was found to be 44 mm at 6.0 kV/cm bias field strength (actuator dimensions: 30 mm in length, 8 mm in width and 1.3 mm in thickness). The maximum tip displacement of the 3:1

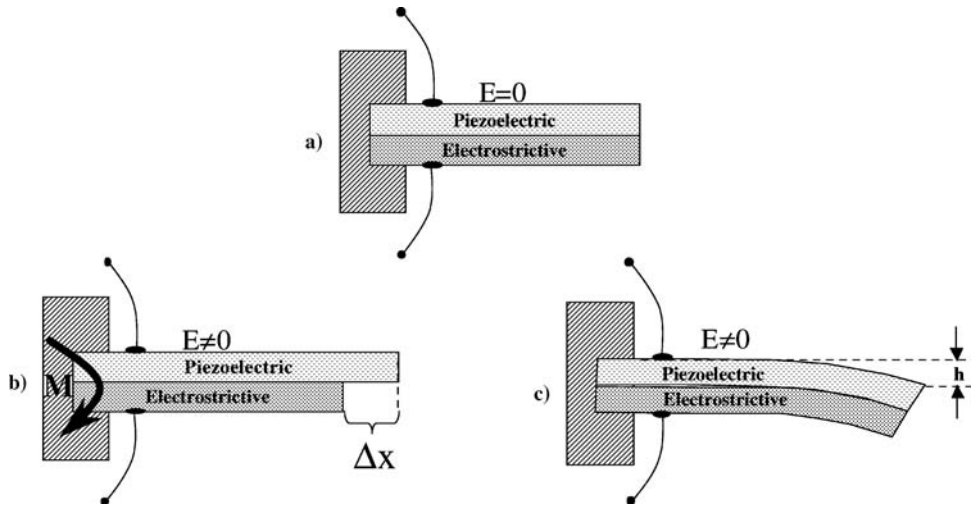

Figure 25 (a) Typical bender configuration used in this study, (b) Application of an electric field causes a transverse differential strain Δx (c) Transverse differential strain caused by tip deflection.

monomorph actuator was 76 mm at 6 kV/cm, which corresponds to 50% increase with respect to the 1:1 monomorph. It is interesting to note that the hysteresis of the 3:1 monomorph is also much less in comparison to the 1:1 despite its higher piezoelectric volume fraction, indicating that it would provide for a better positioning accuracy. The tip displacement of the 1:3 monomorph is the smallest of the three, with a maximum at ∼20 mm at 6 kV/cm. The aforementioned comparison indicates that the tip displacement in such monomorph actuators can substantially be increased by clamping the transverse displacement of the piezoelectric with an electrostrictive layer that is lower in volume fraction. The electrostrictive layer also imparts lower hysteresis to the actuators, which is desirable in regard to positioning precision. In principle, one should be able to further increase the tip displacement, while at the same time reducing the hysteresis by decreasing the thickness of the electrostrictive layer.

Oval actuators

Monolithic piezoelectric actuators with oval geometry have been prototyped by FDC and characterized for applications such as fluid delivery systems as depicted in Fig. 27 [107]. The minor diameter of the ovals varied between 2 and 14 mm, and their major diameter, wall thickness, and width were 20, 0.85, and 7 mm, respectively. When driven under electric field, the actuators expanded along their minor diameter. The static and dynamic displacements of 7 and 5.6 mm were observed at 850 V DC and 100 V AC. The static displacement of the ovals varied almost linearly with voltage and did not change under the application of external load in the range of 1–15 N [107]. Fig. 27 displays the effect of minor diameter on the displacement of ovals at their resonance frequency driven under a 100 V AC sinusoidal excitation at 50 Hz [107]. As seen, the ovals with 4 mm minor diameter had the maximum displacement of 5.6 mm. The displacement at 100 V is notably amplified ∼7 times at the resonance frequency. Such amplification is important for applications in piezoelectric motors where actuators usually operate in their resonance mode. As the minor diameter increases above 4 mm, the displacement decreases. From the geometric point of view, an oval gradually transforms into a tube when the minor diameter approaches the major diameter. In a tube, the actuation is attributed to the expansion and contraction of the wall thickness due to the contribution of the d_{31} and d_{33} coefficients. Thus similar to a tube, the displacement of the oval actuators is attributed to the contribution of the d_{31} and d_{33} coefficients. This denotes that when the displacement is in the range 4–14 mm, a nonuniform stress develops due to the effect of d_{31} coefficient

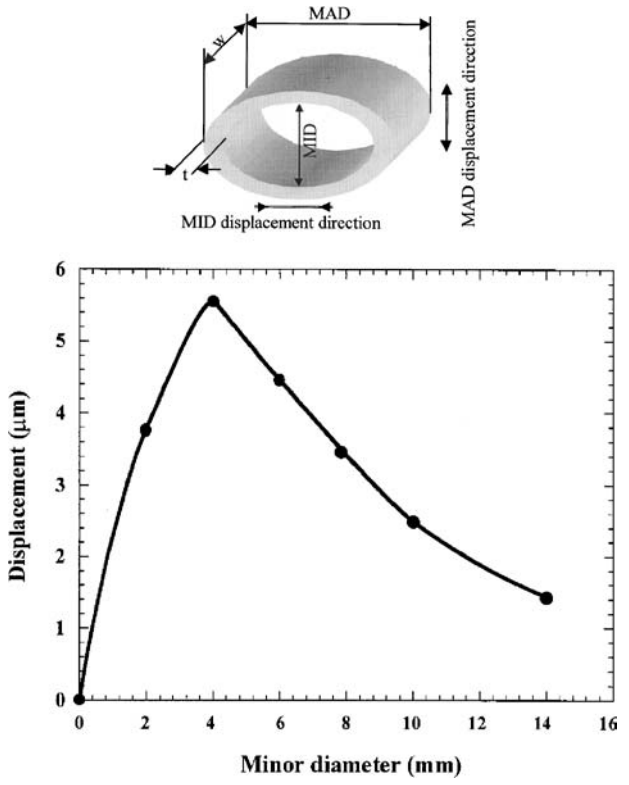

Figure 27 Schematic of Oval Actuators with minor and major diameter (MID and MAD), and the effect of effect of minor diameter on the displacement of ovals at their resonance frequency driven under 100 V ∼ac sinusoidal wave at 50 Hz.

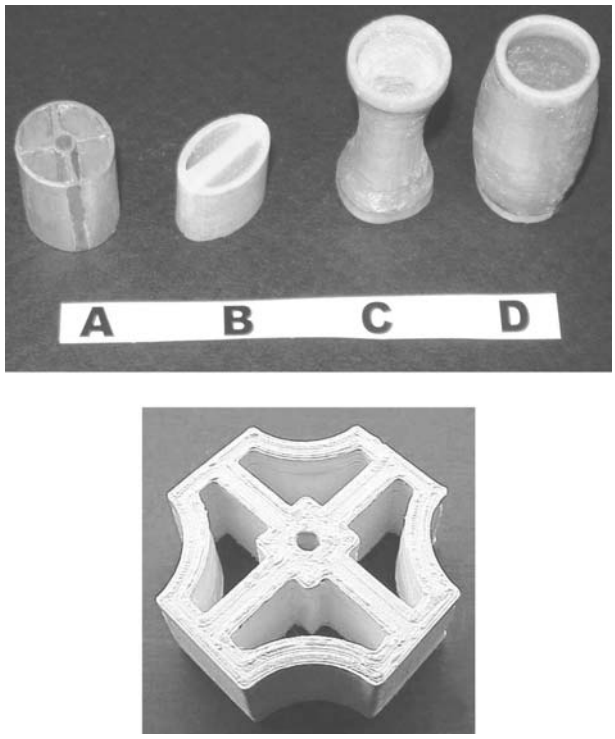

Figure 28 Monolithic multimode transducers with different designs: A. Wagon-Wheel (extruded), B. Class IV (FDC), C. Concave Class I (FDC), D. Convex Class I (FDC) and a Class VII design (bottom).

that creates a bending moment and actuation. When the minor diameter decreases below 4 mm, the displacement again decreases. This suggests that the oval structure behaves similar to a flat ceramic and therefore the bending contribution, as a result of the d_{31}, coefficient becomes less pronounced [107].

New monolithic multimode transducers

Recently, an array of novel multi-mode monolithic piezoelectric transducers has been fabricated using the FDC process [108]. Fig. 28 shows the photographs of some of the prototyped multimode transducers, which include flextensional transducers such as the Wagon Wheel, Class IV, Concave Class I, and Convex Class I, and vector sensors (projectors) [108]. These transducer designs possess internal displacement and/or stress amplification mechanisms that allow tuning of the resonance frequencies and optimization of the vibration modes. In addition, the monolithic nature of the transducers and the flexibility to driving each segment of the transducers separately or in tandem allow one to tune the bandwidth, acoustic radiation beam pattern, and directional response in an unprecedented fashion [108].

5. Summary

There have been great developments in fabrication of piezoelectric ceramic-polymer composites in the last two decades, which were summarized in the paper. The dice and fill method as well as recent fabrication methods, such as injection molding, the relic process, jet machining and the lost mold techniques, are methods with much to offer to composite making. Fused deposition of ceramics (FDC) is an effective technique to further develop piezocomposite technology as demonstrated by the fabrication of "ladder" and "3-D Honeycomb" composites with (3-3) connectivity and oriented (2-2) and (3-3) piezocomposites among others. The indirect and direct methods were both shown to be suitable for making composites. These processes start with a CAD file for the desired part and/or mold. In the indirect method, a CAD file for the negative of the final part is created, while the direct method uses directly deposit the final part. Excellent electromechanical properties for transducer applications have been obtained by these techniques. In addition, the FDC technique clearly shows the ability to form composites with controlled phase periodicity to vary volume fractions and micro and macro-structures, which are not possible with the traditional techniques.

Fused deposition of ceramics has also been used to make an array of novel actuators in the last decade. The flexibility of the FDC system allows for rapid fabrication of parts with frequent change of dimensions for optimization purposes. Actuators such as tubes with straight, bellows, and curved wall geometry, spirals, telescoping, ovals, and monomorphs have been prototyped and characterized. Spiral actuators show large tangential displacements with moderate blocking force. Monomorph piezoelectric/electrostrictive PMN-PT bender is a novel design with large tip deflection. By varying the ratio of the piezoelectric to electrostrictive layer, it is feasible to optimize the field-induced strain of the actuator for a given application. SFF technology is a great tool for rapid prototyping of new designs and verification of modeling.

Acknowledgments

We wish to thank for the generous financial support provided by the Office of Naval Research (ONR), the Defense Advanced Research Projects Agency (DARPA), and New Jersey Commission on Science and Technology (NJCTS). The contributions of S. C. Danforth, N. Langrana, M. Jafari, S. Guceri, and T.-W. Chou to the SFF work presented herein is gratefully acknowledged. We also wish to thank the past members of the Electroceramics Research Group at Rutgers University, A. Bandhophadhyay, R. K. Panda, T. F. McNulty, S. Turcu, G. Lous, F. Mohammadi, and B. Jadidian, whose work is summarized in this article.

References

1. K. UCHINO, in "Piezoelectric Actuators and Ultrasonic Motors" (Kluwer Academic Publisher, New York, 1996).
2. B. JAFFE, W. R. COOK and H. JAFFE, in "Piezoelectric Ceramics" (R.A.N. Publishers, Marietta, Ohio, 1971).
3. Y. XU, in "Ferroelectric Materials and Their Applications" (North-Holland, Amsterdam, 1991).
4. L. E. CROSS, in "Ferroelectric ceramics: Tailoring properties for specific applications," edited by N. Setter and E. L. Colla. (Birkhauser, Basel, 1993).
5. G. GOODMAN, *J. Amer. Ceram. Soc.* **36** (1960) 368.
6. E. C. SUBBARAO, *ibid.* **43** (1960) 439.
7. G. Y. XU, Z. ZHONG, Y. BING, Z. G. YE, C. STOCK and G. SHIRANE, *Phys. Rev.* **B 67** (2003) 104102.
8. Z. G. YE, Y. BING, J. GAO, A. A. BOKOV, P. STEPHENS, B. NOHEDA and G. SHIRANE, *Phys. Rev.* **B 67** (2003) 104104.
9. H. M. JI, Z. BING and M. X. XU, *Rare Metal Mater. Eng.* **31** (2002) 292.
10. Y. H. BING, R. GUO and A. S. BHALLA, *Ferroelectrics* **242** (2000) 1.
11. Y. H. BING and Z. G. YE, *J. Cryst. Growth* **250** (2003) 118.
12. N. YASUDA, N. UEMURA, H. OHWA, Y. YAMASHITA, M. IWATA, M. MAEDA, I. SUZUKI and Y. ISHIBASHI, *J. Korean Physical Soc.* **42** (2003) S1261.
13. M. IWATA, N. TOMISATO, H. ORIHARA, H. OHWA, N. YASUDA and Y. ISHIBASHI, *Ferroelec.* **261** (2001) 747.
14. M. IWATA, N. TOMISATO, H. ORIHARA, N. ARAI, N. TANAKA, H. OHWA, N. YASUDA and Y. ISHIBASHI, *Jpn. J. Appl. Phys. Part 1* **40** (2001) 5819.
15. H. OHWA, M. IWATA, H. ORIHARA, N. YASUDA and Y. ISHIBASHI, *J. Phys. Soc. Jpn.* **70** (2001) 3149.
16. R. E. EITEL, C. A. RANDALL, T. R. SHROUT and S. E. PARK, *Jpn. J. Appl. Phys. Part 1* **41** (2002) 2099.
17. S. J. ZHANG, L. LEBRUN, S. RHEE, R. E. EITEL, C. A. RANDALL and T. R. SHROUT, *J. Crys. Growth* **236** (2002) 210.

18. S. J. ZHANG, P. W. REHRIG, C. RANDALL and T. R. SHROUT, *ibid.* **234** (2002) 415.
19. S. J. ZHANG, S. RHEE, C. A. RANDALL and T. R. SHROUT, *Jpn. J. Appl. Phys. Part 1* **41** (2002) 722.
20. S. J. ZHANG, C. A. RANDALL and T. R. SHROUT, *Appl. Phys. Lett.* **83** (2003) 3150.
21. L. E. CROSS, *Nature* **432**(4) (2004) 84 (and references cited therein).
22. D. P. SKINNER, R. E. NEWNHAM and L. E. CROSS, *Mat. Res. Bull.* **13** (1978) 599.
23. R. E. NEWNHAM, *Ferroelec.* (1986) 1.
24. H. P. SAVAKUS, K. A. KLICKER and R. E. NEWNHAM, *Mater. Res. Bull.* **16** (1981); KLICKER, Ph.D. Thesis. (The Pennsylvania State University, 1980).
25. J. W. SLIWA, S. AYTER and J. P. MOHR, U. S. Pat. No. 5239736, 1993.
26. R. L. GENTILMAN, D. F. FIORE, H. T. PHAM, K. W. FRENCH and L. J. BOWEN, in "Ceramic Transactions, Ferroic Materials: Design, Preparation, and Characteristics", edited by A. S. Bhalla, K. M. Nair, I. K. Lloyd, H. Yanagida and D. A. Payne. (American Ceramic Society, Westerville, OH, 1994), Vol. 43: 239.
27. L. J. BOWEN and K. W. FRENCH, IEEE *Proceedings of the Int'l Symp. on the Appl. of Ferroelec.* (1992), 160.
28. L. J. BOWEN, R. L. GENTILMAN, H. T. PHAM, D. F. FIORE and K. W. FRENCH, in Proceedings of the IEEE Ultrasonics Symposium (1993), 499.
29. R. L. GENTILMAN, D. FIORE, H. PHAM, W. SERWATKA and L. BOWEN, in Proceedings of the SPIE: Industrial and Commercial Applications of Smart Structures Technologies, Vol. 2447, (1995) p. 274.
30. W. WERSING, in Proceedings IEEE International Symposium on Applications of Ferroelectrics (1986) p. 212.
31. E. W. BECKER, W. EHRFELD, P. HAGMANN, A. MANER and D. MUNCHMEYER, *Microelec. Eng.* **4** (1986) 35.
32. U. BAST, D. CRAMER and A. Wolff, in Ceramics Today-Tomorrow's Ceramics, edited by. P. Vincenzini. (Elsevier Science Publishers, Amsterdam, 1991), Vol. 66C.
33. U. BAST, H. KAARMANN, K. LUBITZ, M. VOGT, W. WERSING and D. CRAMER, U.S. Patent No. 5164920 (1992).
34. K. LUBITZ, A. WOLFF and G. PREU, *Ferroelec.* **133** (1992).
35. K. LUBITZ, A. WOLFF and G. PREU, in IEEE Ultrasonics Symposium (Piscataway, New Jersey, 1993).
36. K. LUBITZ, A. WOLFF and B. SCHULMEYER, *Ferroelec.* **133** (1992) 21.
37. K. A. LUBITZ, A. WOLFF and G. PREU, Proc. 1993 IEEE Ultrasonics Symposium (Piscataway, New Jersey, 1993).
38. D. J. WALLER, M. S. Thesis, Rutgers University, New Brunswick, NJ (1991).
39. D. J. WALLER, A. SAFARI and R. J. CARD, Proc. of the 7th IEEE Int'l Symp. on the Appl. of Ferroelectr., IEEE, (Piscataway, NJ, USA, 1990) p. 82.
40. J. ZOLA, U.S. Patent No. 4572981 (1986).
41. S. LIVNEH, V. F. JANAS and A. SAFARI, *J. Am. Ceram. Soc.* **78** (1995) 1900.
42. D. J. WALLER, T. IQBAL and A. SAFARI, *ibid.* **72** (1989) 322.
43. S. S. LIVNEH, S. M. TING and A. SAFARI, *Ferroelec.* **157** (1994) 421.
44. J. W. STEVENSON, M. R. REIDMEYER and W. HEUBNER, *J. Am. Ceram. Soc.* **77** (1994) 2491.
45. C. A. RANDALL, D. V. MILLER, J. H. ADAIR and A. S. BHALLA, *J. Mater. Res.* **8** (1993) 899.
46. C. A. RANDALL, C. P. BOWEN, T. R. SHROUT, A. S. BHALLA and R. E. NEWNHAM, in Proceedings of the 6th U.S. Japan Seminar on Dielectric and Piezoelectric Ceramics (1993) p. 152.
47. M. EYETT, D. BAUERLE and W. WERSING, *J. Appl. Phys.* **62** (1987) 1511.
48. Y. OHARA, M. MIYAYAMA, K. KOUMOTO and H. YANAGIDA, *Sensors and Actuators A* **40** (1994) 345.
49. *Idem.*, *J. Mater. Sci. Lett.*, **12** (1993) 1279.
50. M. J. CREEDON, S. GOPALAKRISHAN and W. A. SCHULZE, IEEE International Symposium on the Application of Ferroelectrics (State College, PA, 1994).
51. M. J. CREEDON and W. A. SCHULZE, *Ferroelec.* **153** (1994) 333.
52. J. D. ERVIN, D. BREI, C. A. V. HOY, J. R. MAWDSLEY and J. W. HALLORAN, in Proceedings of the ASME Aerospace Division (1996), Vol. 52, pp. 695–697.
53. C. A. V. HOY, A. BARDA, M. GRIFFITH and J. W. HALLORAN, *J. Am. Ceram. Soc.* **81** (1998) 152.
54. D. P. SKINNER, R. E. NEWNHAM and L. E. CROSS, *Mat. Res. Bull.* (1978) 1553.
55. K. A. KLICKER, W. A. SHULTZE and J. V. BIGGERS, *J. Am. Ceram. Soc.* **65** (1982) C208.
56. K. RITTENMYER, T. SHROUT, W. A. SCHULZE and R. E. NEWNHAM, *Ferroelec.* **41** (1982) 323.
57. Materials System Inc., www.matsysinc.com, (2004).
58. W. HACKENBERGER, P. MING-JEN, D. KUBAN, T. RITTER and T. SHROUT, Novel method for producing high frequency 2-2 composites from PZT ceramic, in IEEE Proceedings of the Ultrasonics Symposium, (2000), Vol. 2, pp. 969.
59. R. P. SCHAEFFER, V. F. JANAS and A. SAFARI, Proceedings of the 10th IEEE International Symposium on Applications of Ferroelectrics, Part 2 of 2 (1996).
60. W. HUEBNER, M. R. REIDMEYER, J. W. STEVENSON and L. BUSSE, Proceedings of the 9th IEEE International Symposium on Applications of Ferroelectrics (University Park, PA, USA, 1994).
61. D. M. MILLS and S. W. SMITH, *IEEE Transactions of the Ultrasonics, Ferroelectrics and Frequency Control.* **49** (2002) 1005.
62. C. VAN HOY, A. BARDA, M. GRIFFITH and J. W. HALLORAN, *J. Amer. Ceramic Soc.* **81** (1998) 152.
63. J. W. HALLORAN, *Brit. Ceramic Trans.* **98** (1999) 299.
64. H. L. MARCUS, J. J. BEAMAN, J. W. BARLOW, D. L. BOURELL and R. H. CRAWFORD, Solid Freeform Fabrication Symposium, (Austin, TX, 1992).
65. H. L. MARCUS, J. J. BEAMEN, J. W. BARLOW, D. L. BOURELL and R. H. CRAWFORD, Solid Freeform Fabrication Proceedings (Austin, TX, 1992).
66. H. L. MARCUS, J. J. BEAMEN, J. W. BARLOW, D. L. BOURELL and R. H. CRAWFORD, Solid Freeform Fabrication Proceedings, (University of Texas at Austin, Austin, TX, 1991).
67. H. L. MARCUS and D. L. BOURELL, *Adv. Mat. Proc.* **9** (1993) 677.
68. H. L. MARCUS, *Mech. Eng.* **117** (1995) 62.
69. D. L. BOURELL, J. J. BEAMEN, H. L. MARCUS and J. W. BARLOW, Solid Freeform Fabrication Proceedings (Austin, TX, 1990).
70. P. F. JACOBS, "Stereolithography and Other RP & M Technologies from Rapid Prototyping to Rapid Tooling," Dearborn, MI: Society of Manufacturing Engineers (1995).
71. P. F. JACOBS, "Rapid Prototyping & Manufacturing: Fundamentals of StereoLithography," Dearborn, MI: Society of Manufacturing Engineers (1992).
72. M. FEYGIN and B. HSIEH, in Proceedings of the Solid Freeform Fabrication Symposium. (1991), p. 123.
73. M. FEYGIN, U. S. Patent No. 5354414 (1994).
74. J. CESARANO, T. A. BAER and P. CALVERT, in Proceedings of the Solid Freeform Fabrication Symposium. (1997) Vol. 8, pp. 25.

75. J. CESARANO, B. H. KING and H. B. DENHAM, in Proceedings of Solid Freeform Fabrication Symposium, (1998) Vol. 9, pp. 697.
76. E. M. SACHS, M. J. CIMA, P. WILLIAMS, D. BRANCAZIO and J. CORNIE, *J. Eng. Ind.* **114** (1992) 481.
77. R. K. PANDA, Ph.D. Thesis, Rutgers University, New Brunswick, New Jersey (1998).
78. J. CESARANO and P. CALVERT, U.S. Patent No. 6027326 (2000).
79. A. SAFARI, Ph.D. Thesis, The Pennsylvania State University, State College, PA (1983).
80. W. SCHULZE, *Ferroelectrics* **50** (1983) 33.
81. T. R. SHROUT, L. J. BOWEN and W. A. SCHULZE, *Mater. Res. Bulletin* **15** (1980) 1371.
82. A. SAFARI, *ibid.* **17** (1982) 301.
83. S. TURCU, M.S. Thesis, Rutgers University, New Brunswick, NJ (2002).
84. S. TURCU, B. JADIDIAN, S. C. DANFORTH and A. SAFARI, *J. Electroc.* **9** (2002) 165.
85. C. W. NAN, L. LIU and L. LI, *J. Phys. D* **33** (2000) 2988.
86. C. W. NAN and G. W. WENG, *J. Appl. Phys.* **88** (2000) 416.
87. A. BANDYOPADHYAY, R. K. PANDA, V. E. JANAS, M. K. AGARWALA, S. C. DANFORTH and A. SAFARI, *J. Amer. Ceramic Society* **80** (1997) 1366.
88. A. SAFARI, V. F. JANAS and R. K. PANDA, SPIE Symposium on Smart Structures and Materials, (San Diego, CA, 1996).
89. A. SAFARI, J. CESARANO, P. G. CLEM and B. BENDER, Proceedings of the 13th IEEE International Symposium on Applications of Ferroelectronics, (Nara, Japan, 2002).
90. G. H. HAERTLING, *Am. Ceram. Soc. Bull.* **73** (1994) 93.
91. F. MOHAMMADI, A. KHOLKIN, B. JADIDIAN and A. SAFARI, *Appl. Phys. Lett.* **75** (1999) 2488.
92. Q. M. WANG, Q. ZHANG, B. XU, R. LIU and L. E. CROSS, *J. Appl. Phys.* **86** (1999) 3352.
93. A. SAFARI, S. C. DANFORTH, M. A. JAFARI, M. ALLAHVERDI, B. JADIDIAN, F. MOHAMMADI, N. VANKATARAMAN and S. RANGARAJAN, in Proceedings of the 9th European Conference on Rapid Prototyping and Manufacturing, (2000) p. 247.
94. A. SAFARI and S. C. DANFORTH, in Proceedings of the 11th IEEE International Symposium on the Applications of Ferroelectrics, (1998) p. 229.
95. A. BANDYOPADHYAY, R. K. PANDA, T. F. MCNULTY, F. MOHAMMADI, S. C. DANFORTH and A. SAFARI, *Rapid Prototyping Journal* **4** (1998) 37.
96. A. SAFARI and M. ALLAHVERDI, *Ceram. Eng. Sci. Proc.* **22** (2001) 473.
97. F. MOHAMMADI, Ph.D. Thesis, Department of Ceramic and Materials Engineering, Rutgers University, New Jersey, USA (2001).
98. F. MOHAMMADI, A. KHOLKIN, S. C. DANFORTH and A. SAFARI, in Proceedings of the 11th IEEE International Symposium on the Applications of Ferroelectrics, pp. 273–275 (1998).
99. S. A. WISE, *Sensors and Actuators A* **69** (1998) 33.
100. Q. M. ZHANG, H. WANG and L. E. CROSS, *J. Mater. Sci.* **28** (1993) 3962.
101. Y. SUGAWARA, K. ONITSUKA, S. YOSHIKAWA, Q. C. XU, R. E. NEWNHAM and K. UCHINO, *J. Am. Ceram. Soc.* **75** (1992) 996.
102. A. M. UMARJI, A. L. KHOLKIN, T. F. MCNULTY, S. C. DANFORTH and A. SAFARI, in Proceedings of the 11th IEEE International Symposium on the Applications of Ferroelectrics, (1998) p. 269.
103. T. W. CHOU, B. A. CHEESEMAN, A. SAFARI and S. C. DANFORTH, *Ceramic Eng. Sci. Proc.* **22** (2001) 497.
104. J. CHEN, Q. M. ZHANG, L. E. CROSS and C. M. TROTTIER, in Proceedings of International Conference on Intelligent Materials (ICIM), Williamsburg, VA, pp. 316–318 (1994).
105. M. ALLAHVERDI and A. SAFARI, *J. Eur. Ceram. Soc.* **21** (2001) 1485.
106. M. ALLAHVERDI, B. JADIDIAN, B. HARPER, S. RANGARAJAN, M. JAFARI, S. C. DANFORTH and A. SAFARI, in Proceedings of 12th IEEE International Symposium on Applications of Ferroelectrics, edited by S. K. Streiffer, B. J. Gibbons and T. Tsurumi, (IEEE-UFFC, New Jersey, 2001) p. 381.
107. B. JADIDIAN, M. ALLAHVERDI, F. MOHAMMADI and A. SAFARI, *Appl. Phys. Lett.* **80** (2002) 1981.
108. R. E. NEWNHAM, D. C. MARKLEY, R. J. MEYER JR, W. J. HUGHES, A.-C. HLADKY-HENNION and J. K. COCHRAN JR, *Ceramic Transactions* **150** (2004) 427.